CELLULAR NEUROSCIENCE

Deficient chaperone-mediated autophagy facilitates LPS-induced microglial activation via regulation of the p300/NF-κB/NLRP3 pathway

Jin Wu[1], Yingying Han[1], Hao Xu[1], Hongyang Sun[1], Rui Wang[1], Haigang Ren[1]*, Guanghui Wang[1,2]*

Neuroinflammation is a pathological change that is involved in the progression of Parkinson's disease. Dysfunction of chaperone-mediated autophagy (CMA) has proinflammatory effects. However, the mechanism by which CMA mediates inflammation and whether CMA affects microglia and microglia-mediated neuronal damage remain to be elucidated. In the present study, we found that LAMP2A, a limiting protein for CMA, was decreased in lipopolysaccharide (LPS)–treated primary microglia. Activation of CMA by the activator CA significantly repressed LPS-induced microglial activation, whereas CMA dysfunction exacerbated microglial activation. We further identified that the protein p300 was a substrate of CMA. Degradation of p300 by CMA reduced p65 acetylation, thereby inhibiting the transcription of proinflammatory factors and the activation of the NLRP3 inflammasome. Furthermore, CA pretreatment inhibited microglia-mediated inflammation and, in turn, attenuated neuronal death in vitro and in vivo. Our findings suggest repressive effects of CMA on microglial activation through the p300-associated NF-κB signaling pathway, thus uncovering a mechanistic link between CMA and neuroinflammation.

INTRODUCTION

Parkinson's disease (PD), the second most common neurodegenerative disease following Alzheimer's disease (AD), is characterized by the loss of dopaminergic (DA) neurons and the accumulation of Lewy bodies in the substantia nigra pars compacta (SNpc) (*1*–*3*). Clinically, patients show motor symptoms of bradykinesia, rigidity, resting tremor, and postural instability, as well as nonmotor symptoms of constipation, depression, sleep disorders, and cognitive decline (*4*, *5*). Although the pathological mechanisms of PD are largely unknown, accumulating evidence suggests that neuroinflammation greatly contributes to the progression of PD, especially in the early stages of disease (*6*, *7*). Hyperactivated microglia are a major source for the production of proinflammatory cytokines, such as interleukin-6 (IL-6), IL-1β, and tumor necrosis factor–α (TNF-α), which lead to subsequent DA neuronal degeneration (*8*). The activation of microglia is present in postmortem PD brains and PD model animals (*9*–*11*).

Although the mechanisms by which microglia are activated in PD remain to be investigated, a number of signaling pathways have been identified to trigger inflammatory responses. Among them, the nuclear factor κB (NF-κB) pathway plays a key role in activating inflammation (*12*–*14*). Upon stimulation with lipopolysaccharide (LPS), the transcription factor NF-κB/p65 enters the nucleus to transactivate genes that express proinflammatory cytokines and NLR family pyrin domain containing 3 (NLRP3), a core protein of the NLRP3 inflammasome (*15*, *16*).

Chaperone-mediated autophagy (CMA) is a process that targets specific soluble proteins for lysosomal degradation. All CMA substrates have at least one Lys-Phe-Glu-Arg-Gln (KFERQ)–like motif that is recognized by the cytosolic chaperone heat shock cognate protein 70 (HSC70) (*17*, *18*). Coordinated by HSC70, substrate proteins are bound to lysosome-associated membrane protein type 2A (LAMP2A) and translocated into the lysosome for degradation (*19*). Under physiological conditions, CMA activation removes oxidized and damaged proteins to maintain proteostasis and prevent cell death under conditions such as starvation, hypoxic stress, and endoplasmic reticulum stress (*20*–*23*). CMA dysfunction is closely related to many neurodegenerative diseases, such as PD and AD (*24*, *25*). The PD-related proteins—α-synuclein, leucine-rich repeat kinase 2 (LRRK2), and DJ-1—have been identified as typical substrates of CMA (*26*–*28*). LAMP2A, a core component of CMA, is significantly decreased in early PD, accompanied by an increase in α-synuclein levels (*29*). In addition, the protein levels of HSC70, another core component of CMA, are decreased in peripheral blood mononuclear cells of patients with PD (*30*), suggesting that the dysregulation of CMA may occur in the progression of PD. It has been well documented that CMA activation protects DA neurons in cell and animal models of PD (*31*–*33*). However, the relationship between CMA and immune responses in microglia and the mechanism by which CMA influences microglial activation remain largely unknown.

In the present study, we demonstrated that LAMP2A deficiency exacerbates microglial activation, while the CMA activator CA markedly inhibits microglial activation and protects DA neurons from inflammation-induced cell death in vitro and in vivo. Moreover, we found that the p300/NF-κB/NLRP3 signaling pathway is involved in the CMA-mediated regulation of neuroinflammation.

[1]Laboratory of Molecular Neuropathology, Department of Pharmacology, Jiangsu Key Laboratory of Neuropsychiatric Diseases and College of Pharmaceutical Sciences, Soochow University, Suzhou 215123, Jiangsu, China. [2]MOE Key Laboratory, Soochow University, Suzhou 215123, Jiangsu, China.
*Corresponding author. Email: rhg@suda.edu.cn (H.R); wanggh@suda.edu.cn (G.W.)

RESULTS

CMA dysfunction promotes LPS-induced production of proinflammatory factors in microglia

It is well accepted that LAMP2A is a key limiting factor for CMA. To assess whether CMA dysfunction potentially affects microglial activation, we examined the effects of CMA on the activation of microglia in which *LAMP2A* small interfering RNAs (siRNAs) were transfected into BV2 cells to knock down *LAMP2A*. The siRNAs that target *LAMP2A* (si-*L2A*-1$^{\#}$ and si-*L2A*-2$^{\#}$) effectively decreased LAMP2A protein levels (Fig. 1A) but did not change the expression levels of another two LAMP2 isoforms, *LAMP2B* and *LAMP2C* (Fig. 1B), suggesting a specificity of si-*L2A*. In BV2 cells, LPS significantly induced the expression of inducible nitric oxide (NO) synthase (iNOS) and cyclooxygenase-2 (COX-2) (Fig. 1C). Moreover, knockdown of *LAMP2A* aggravated LPS-induced expression of iNOS and COX-2 (Fig. 1C) and the production of the inflammatory factors NO (Fig. 1D) and IL-6 (Fig. 1E) without affecting cell viability (fig. S1A). In addition, knockdown of *LAMP2A* also aggravated the mRNA expression of *iNOS* (Fig. 1F), *COX-2* (Fig. 1G), *IL-6* (Fig. 1H), and *IL-1β* (Fig. 1I) in BV2 cells that were treated with LPS. Similarly, in primary microglia, LAMP2A silencing also significantly increased the LPS-induced expression of iNOS and COX-2 (Fig. 1J) and the production of NO (Fig. 1K). To further identify the effects of CMA on microglial activation, we constructed a *LAMP2A*-knockout (KO) BV2 cell line using CRISPR-Cas9 technology. KO of *LAMP2A* induced increased expression of iNOS (Fig. 1L) and the production of NO (Fig. 1M) in BV2 cells that were treated with LPS. In addition, KO of *LAMP2A* also aggravated the mRNA expression of *iNOS* (Fig. 1N) in LPS-stimulated BV2 cells.

CMA activation inhibits LPS-induced production of proinflammatory factors in microglia

Because we found that CMA blockade in microglia promoted LPS-induced microglial activation, we wondered whether CMA activation could inhibit LPS-induced production of proinflammatory factors. We used CA77.1 (CA) and QX77, two potent CMA activators that activate CMA by antagonizing retinoic acid receptor α without affecting macroautophagy (*25*, *34*), to investigate the contributions of CMA.

In BV2 cells, CA or QX77 treatment had no effect on cell viability (fig. S1B). Furthermore, pretreatment with CA (Fig. 2A) or QX77 (fig. S2A) significantly decreased LPS-induced expression of iNOS and COX-2. Pretreatment with CA (Fig. 2, B and C) or QX77 (fig. S2, B and C) also decreased LPS-induced production of the proinflammatory factors NO and IL-6. In addition, pretreatment with CA (Fig. 2, D to G) or QX77 (fig. S2, D to G) decreased the mRNA expression of *iNOS*, *COX-2*, *IL-6*, and *IL-1β* in BV2 cells treated with LPS. Similar data were obtained in primary microglia, showing that CA repressed LPS-induced expression of iNOS and COX-2 (Fig. 2H) and production of NO (Fig. 2I). To verify that the anti-inflammatory effects of CA depend on CMA, we examined CA-treated BV2 cells in which *LAMP2A* was knocked down. In BV2 cells that were treated with LPS, CA inhibited the expression of iNOS (Fig. 2J) and the mRNA expression of the proinflammatory factors *IL-6* (Fig. 2K) and *IL-1β* (Fig. 2L). However, knockdown of *LAMP2A* abolished the inhibitory effects of CA on LPS-induced expression of inflammatory factors (Fig. 2, J to L). These data suggest that CMA activation inhibits LPS-induced microglial activation.

CMA negatively regulates LPS-induced NF-κB transcriptional activity

Because we have shown that CMA plays an important role in microglial activation, we wondered how CMA regulates LPS-induced inflammation. Mounting evidence indicates that the activator protein 1 (AP-1) pathway and NF-κB pathway are involved in LPS-induced microglial activation (*35*, *36*). Thus, we first examined whether the repression of inflammation by CMA activation was dependent on the AP-1 pathway. After activation of Toll-like receptor 4 (TLR4) by LPS, mitogen-activated protein kinases, including extracellular signal–regulated kinase (ERK), c-Jun N-terminal kinase (JNK), and p38, are activated to promote the expression and phosphorylation of c-Jun and c-Fos, which form AP-1 dimers, inducing the transcription of proinflammatory genes (*35*). In BV2 cells, neither *LAMP2A* siRNAs (Fig. 3A and fig. S3A) nor CA (Fig. 3B and fig. S3B) treatment changed LPS-stimulated phosphorylation of JNK, ERK, and p38, suggesting that AP-1 signaling is not involved in CMA-mediated anti-inflammatory effects.

Next, we tested another inflammatory signaling pathway, the NF-κB pathway, which is also important for microglial activation. Upon LPS stimulation, cytosolic inhibitor of nuclear factor κBα (IκBα) is phosphorylated by IκB kinase (IKK) kinases and then degraded by the proteasome, resulting in the translocation of NF-κB/p65 from the cytoplasm to the nucleus (*15*). LPS-induced nuclear translocation of NF-κB was not changed after CA treatment in BV2 cells that were subjected to immunofluorescence staining (Fig. 3, C and D) and fractionation assays (Fig. 3E). In addition, in BV2 cells that were transfected with *LAMP2A* siRNAs (Fig. 3F) or treated with CA (Fig. 3G), the LPS-stimulated phosphorylation of p65 and degradation of IκBα remained unchanged. However, using an NF-κB luciferase reporter assay in BV2 cells that stably express reporter genes, LAMP2A deficiency increased LPS-induced NF-κB reporter activity (Fig. 3H). Conversely, CA pretreatment markedly decreased NF-κB reporter activity (Fig. 3I). These data suggest that the transcriptional activity of NF-κB is regulated by CMA. To further confirm that CMA is involved in the NF-κB pathway, we examined the effects of the IKK kinase inhibitor IMD0354 on the expression of inflammatory factors in BV2 cells in which *LAMP2A* was knocked down. In BV2 cells, LAMP2A deficiency aggravated LPS-induced expression of the inflammatory factor iNOS (Fig. 3J). However, the increases in the production of the inflammatory factor iNOS that were induced by LAMP2A deficiency were not observed in cells that were treated with IMD0354 (Fig. 3J), suggesting that CMA functions in the NF-κB pathway to repress microglial activation.

CMA activation inhibits the expression and assembly of the NLRP3 inflammasome in microglia

Inflammasomes play roles in neurodegenerative diseases, cancer, and autoimmune diseases, among which the NLRP3 inflammasome is mostly documented (*16*, *37*). As we found that CMA activation inhibits NF-κB transcriptional activity, we wondered whether CMA activation could prevent the expression and assembly of the NLRP3 inflammasome. In BV2 cells stimulated with LPS, LAMP2A deficiency promoted the transcription of *NLRP3* (Fig. 4A) and *IL-18* (Fig. 4B), while CA pretreatment inhibited LPS-induced expression of *NLRP3* (Fig. 4C) and *IL-18* (Fig. 4D). Furthermore, pretreatment with CA decreased the expression of NLRP3 (Fig. 4E), the cleavage of caspase-1 (Fig. 4E), and the production of active IL-1β (Fig. 4F)

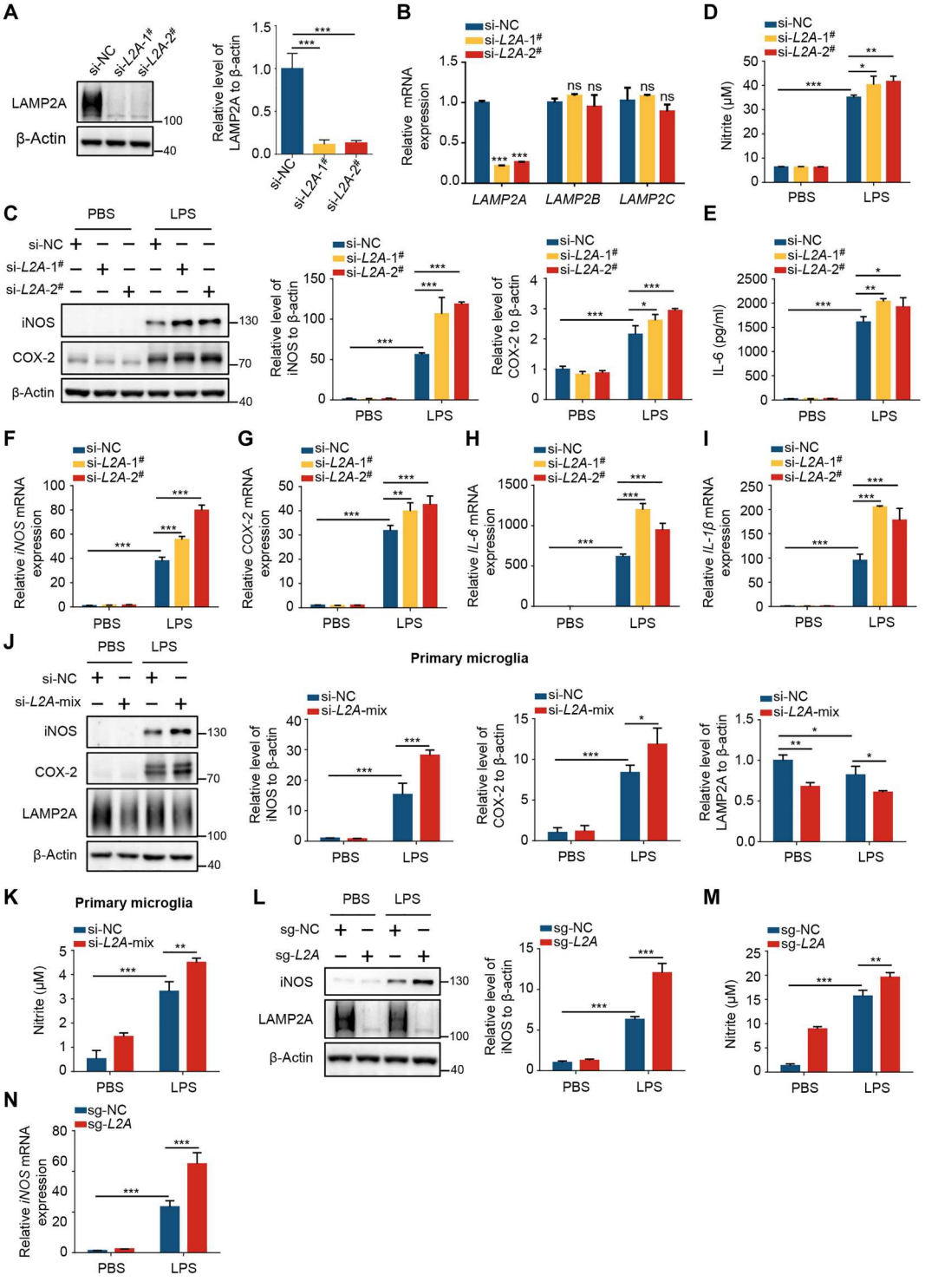

Fig. 1. LAMP2A deficiency promotes LPS-induced production of proinflammatory factors in microglia. (**A** and **B**) Immunoblot analyses with quantification of protein levels of LAMP2A (A), and quantitative polymerase chain reaction (qPCR) analyses of mRNA levels of *LAMP2A*, *LAMP2B*, and *LAMP2C* (B) in BV2 cells that were transfected with control small interfering RNA (siRNA) or *LAMP2A* siRNAs for 72 hours. $n = 3$. (**C** to **I**) Immunoblot analyses with quantification of protein levels of inducible nitric oxide (NO) synthase (iNOS) and cyclooxygenase-2 (COX-2) (C); the quantitative levels of the NO (D) and IL-6 (E) using NO assay kit and enzyme-linked immunosorbent assay (ELISA) kit; and qPCR analyses of mRNA levels of *iNOS* (F), *COX-2* (G), *IL-6* (H), and *IL-1β* (I) in BV2 cells that were transfected with control siRNA or *LAMP2A* siRNAs for 48 hours and then treated with LPS. $n = 3$. (**J** and **K**) Immunoblot analyses with quantification of protein levels of iNOS, COX-2, and LAMP2A (J), and the quantitative levels of the NO using an NO assay kit (K) in primary microglia that were transfected with control siRNA or *LAMP2A* siRNA-mix for 48 hours and then treated with LPS. $n = 3$. (**L** to **N**) Immunoblot analyses with quantification of protein levels of iNOS (L), the quantitative levels of the NO using an NO assay kit (M), and qPCR analyses of mRNA levels of *iNOS* (N) in sg-NC and sg-*LAMP2A* BV2 cells that were treated with LPS. $n = 3$. One-way analysis of variance (ANOVA) followed by Dunnett's multiple comparisons test (A and B) and two-way ANOVA followed by Tukey's multiple comparisons test (C to N).

in primary microglia that were treated with LPS and adenosine 5′-triphosphate (ATP). Similarly, in BV2 cells that were treated with LPS and ATP, immunofluorescence staining for apoptosis-associated speck-like protein containing a CARD (ASC) and enzyme-linked immunosorbent assay (ELISA) assays for IL-1β revealed that pretreatment with CA inhibited the assembly of the NLRP3 inflammasome (Fig. 4, G and H) and the production of active IL-1β (Fig. 4I). These results suggest that CMA activation inhibits the activation of the NLRP3 inflammasome.

p300-mediated p65 acetylation is involved in the anti-inflammatory effect of CMA activation

It has been reported that NF-κB/p65 can be acetylated by p300 at lysine-310 to promote full transcriptional activity in the nucleus

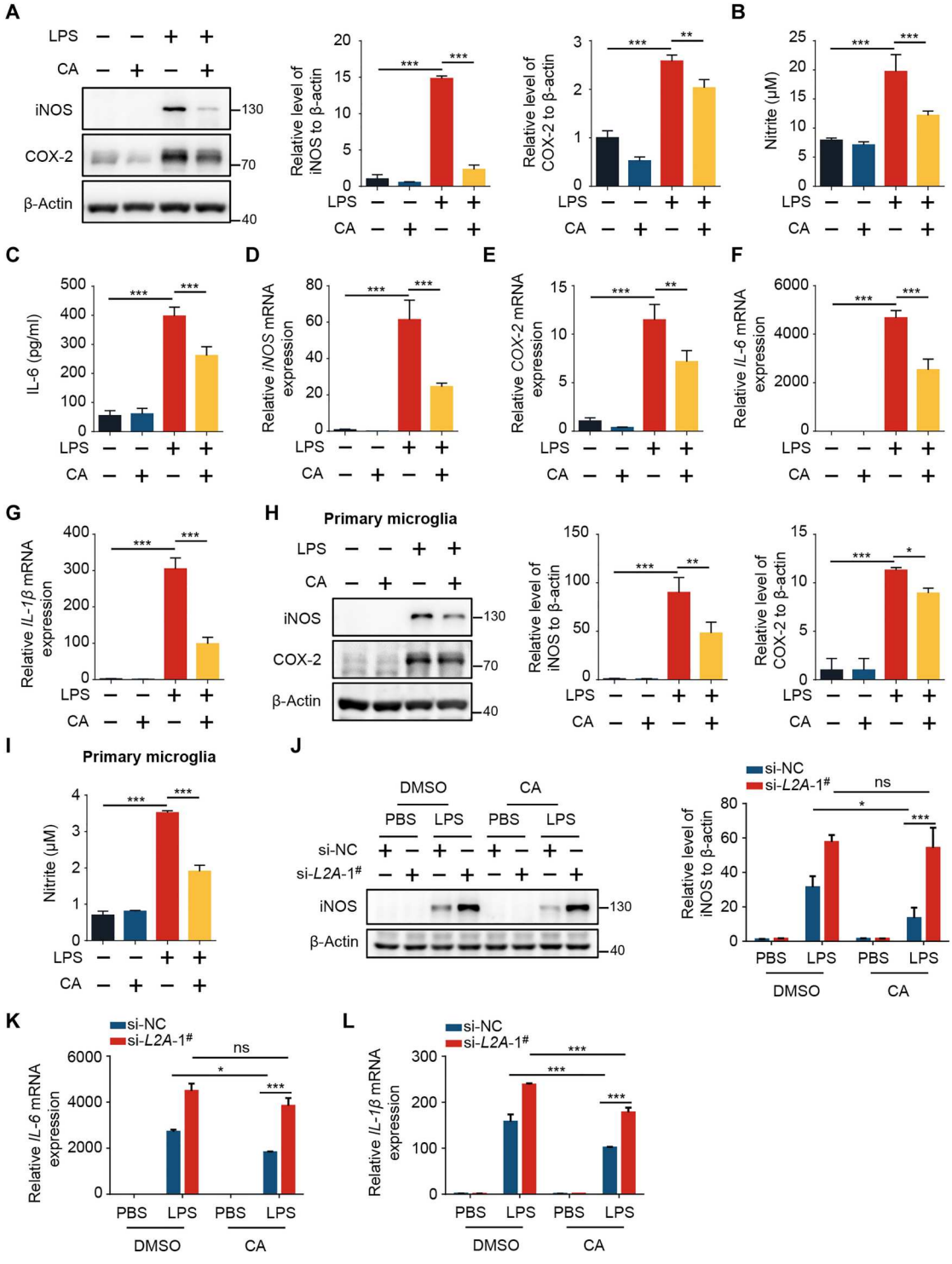

Fig. 2. CMA activators inhibit LPS-induced production of proinflammatory factors in microglia. (**A** to **G**) Immunoblot analyses with quantification of protein levels of iNOS and COX-2 (A); the quantitative levels of the NO (B) and IL-6 (C) using NO assay kit and ELISA kit; and qPCR analyses of mRNA levels of *iNOS* (D), *COX-2* (E), *IL-6* (F), and *IL-1β* (G) in BV2 cells that were pretreated with 12 μM CA, followed by LPS treatment. $n = 3$. (**H** and **I**) Immunoblot analyses with quantification of protein levels of iNOS and COX-2 (H), and the quantitative levels of the NO (I) using an NO assay kit in primary microglia that were treated with 20 μM CA, followed by LPS treatment. $n = 3$. (**J** to **L**) BV2 cells were transfected with control siRNA or *LAMP2A* siRNA for 36 hours, followed by treatment with CA (12 μM) for 12 hours. The cells were then exposed to LPS. Immunoblot analyses with quantification of protein levels of iNOS (J) and qPCR analyses of mRNA levels of *IL-6* (K) and *IL-1β* (L). $n = 3$. One-way ANOVA followed by Dunnett's multiple comparisons test (A to I) and two-way ANOVA followed by Tukey's multiple comparisons test (J to L). DMSO, dimethyl sulfoxide.

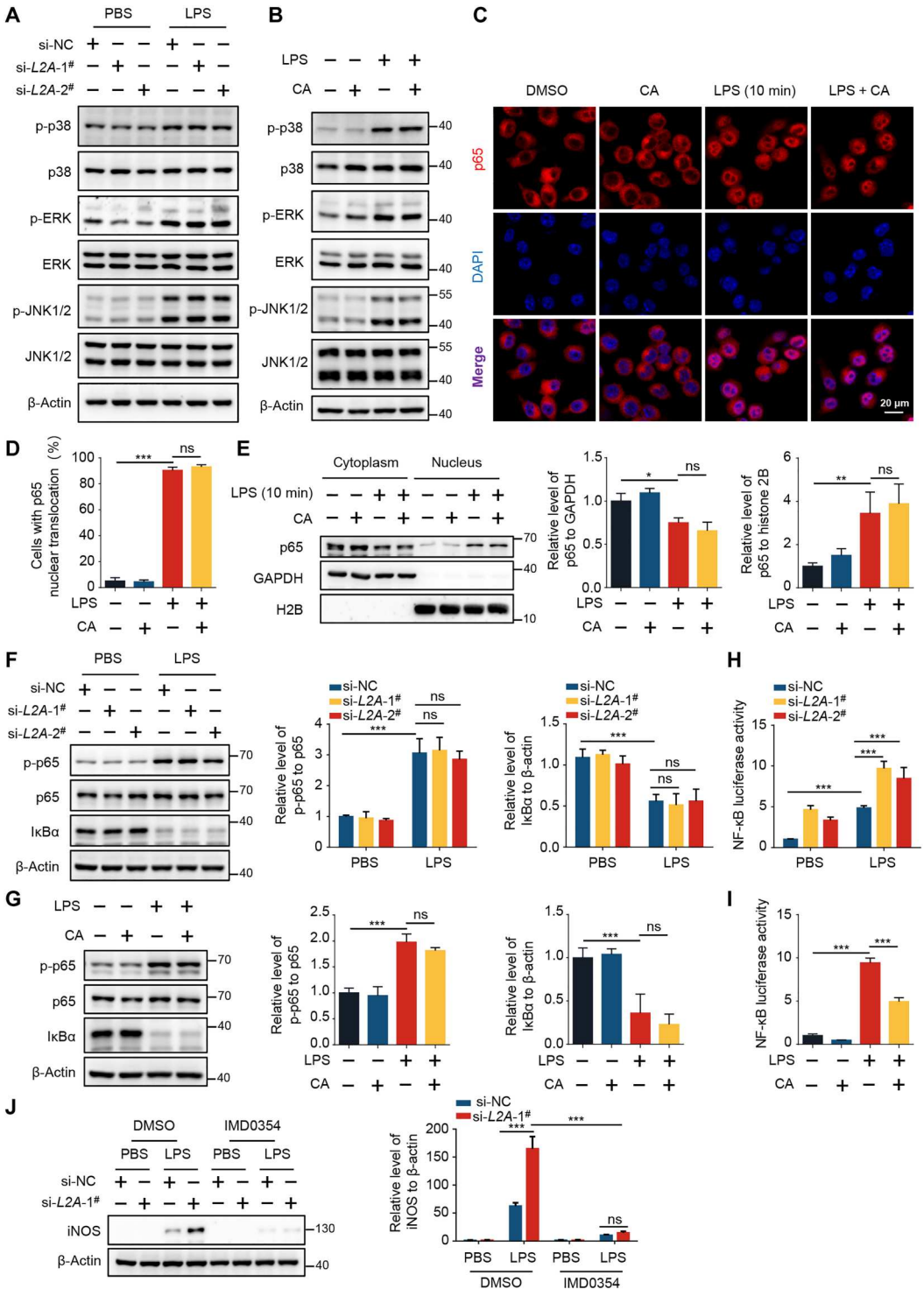

Fig. 3. CMA negatively regulates LPS-induced NF-κB transcriptional activity. (**A** and **B**) Immunoblot analyses of the indicated protein levels in BV2 cells that were transfected with control siRNA or *LAMP2A* siRNAs for 48 hours (A) or pretreated with 12 μM CA for 12 hours (B) and then treated with LPS for 20 min. (**C** to **E**) BV2 cells were pretreated with 12 μM CA for 12 hours and then exposed to LPS for 10 min. Representative images of p65 staining (C). The cells with p65 nuclear translocation were quantified (D). Immunoblot analyses with quantification of protein levels of p65 in the cytoplasm and nucleus using subcellular fractionation assays (E). $n = 3$. (**F** and **G**) Immunoblot analyses with quantification of the indicated protein levels in BV2 cells that were transfected with control siRNA or *LAMP2A* siRNAs for 48 hours (F) or pretreated with 12 μM CA for 12 hours (G) and then treated with LPS for 10 min. $n = 3$. (**H** and **I**) The transcriptional activity of NF-κB was measured with luciferase assays in BV2 cells stably expressing the NF-κB luciferase reporter construct that were transfected with control siRNA or *LAMP2A* siRNAs for 48 hours (H) or pretreated with 12 μM CA for 12 hours (I) and then treated with LPS for 16 hours. $n = 3$. (**J**) BV2 cells were transfected with control siRNA or *LAMP2A* siRNA for 36 hours, followed by treatment with 1.5 μM IMD0354 for 12 hours. The cells were then exposed to LPS for 16 hours. Immunoblot analyses with quantification of protein levels of iNOS. $n = 3$. One-way ANOVA followed by Dunnett's multiple comparisons test (D, E, G, and I) and two-way ANOVA followed by Tukey's multiple comparisons test (F, H, and J).

(*38*, *39*). As we have found that CMA influences NF-κB transcriptional activity but does not affect its nuclear translocation, we wondered whether CMA regulates the acetylation of NF-κB. In BV2 cells, LPS significantly induced the expression of p65 acetylation. Moreover, knockdown of *LAMP2A* aggravated LPS-induced p65 acetylation (Fig. 5A). Conversely, pretreatment with CA decreased LPS-induced p65 acetylation (Fig. 5B). In line with this, pretreatment with CA repressed LPS-induced p65 acetylation in primary microglia (Fig. 5C). To further identify the role of p300 in CMA-mediated p65 acetylation and its relevance to microglial activation, we examined the expression of inflammatory factors using BV2 cells that were treated with *p300* siRNA, p300 antagonists, or a p300 agonist. In BV2 cells, knockdown of *LAMP2A* aggravated LPS-induced expression of iNOS (Fig. 5D and fig. S4A)

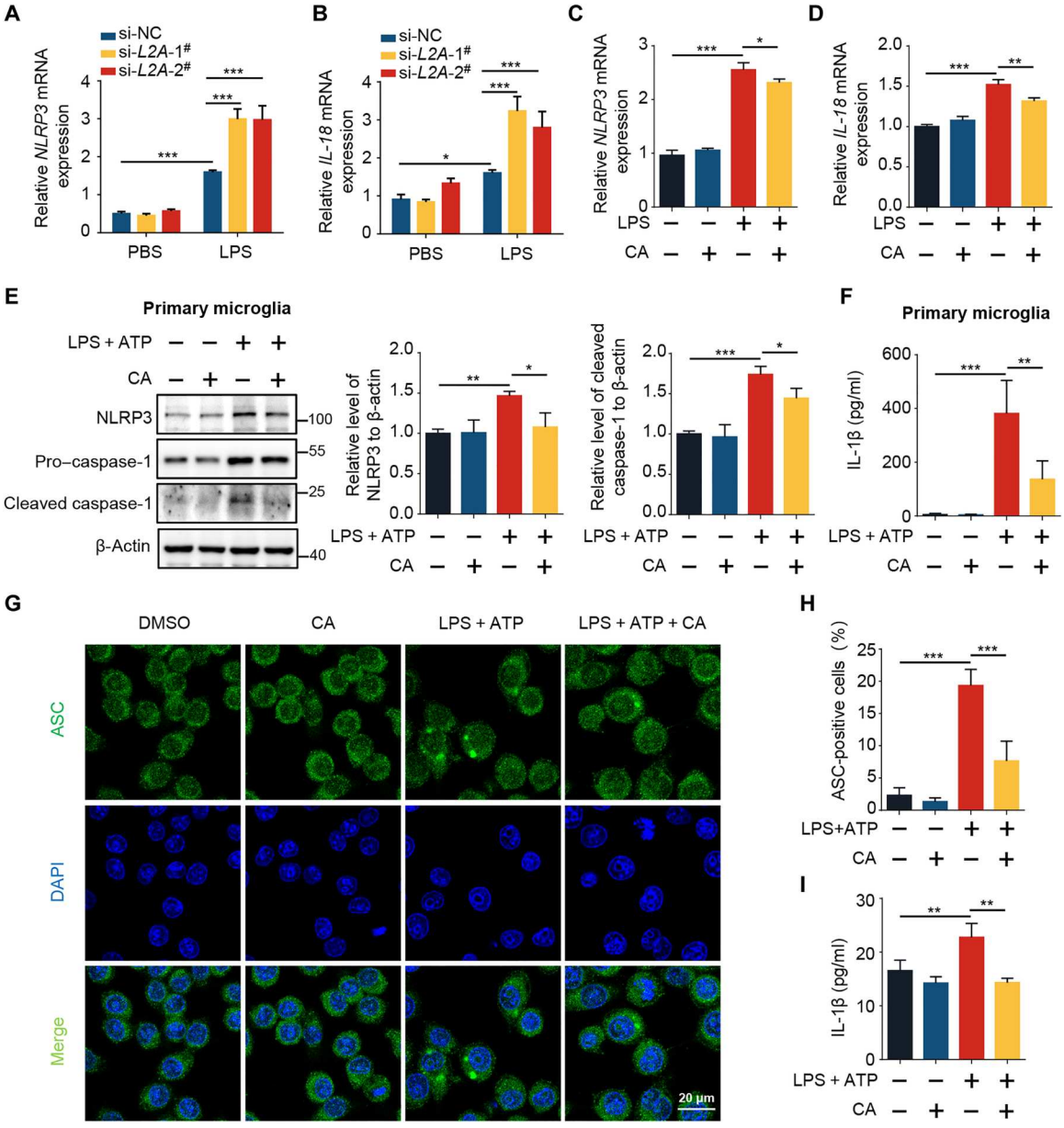

Fig. 4. CMA activation inhibits activation of the NLRP3 inflammasome in microglia. (**A** to **D**) qPCR analyses of mRNA levels of *NLRP3* and *IL-18* in BV2 cells that were transfected with control siRNA or *LAMP2A* siRNAs for 48 hours (A and B) or pretreated with 12 μM CA for 12 hours (C and D) and then treated with LPS for 12 hours. $n = 3$. (**E** and **F**) Primary microglia were pretreated with 20 μM CA for 12 hours and then exposed to LPS for 15 hours and subsequently to adenosine 5′-triphosphate (ATP) (1 mM) for 1 hour. Immunoblot analyses with quantification of the indicated protein levels (E). The quantitative levels of IL-1β were measured using ELISA assays (F). $n = 3$. (**G** to **I**) BV2 cells were pretreated with 12 μM CA for 12 hours and then exposed to LPS for 14 hours and subsequently to ATP (2 mM) for 2 hours. Representative images of ASC staining (G). The cells with ASC puncta were quantified (H). The quantitative levels of IL-1β were measured using ELISA assays (I). $n = 3$. One-way ANOVA followed by Dunnett's multiple comparisons test (C to F, H, and I) and two-way ANOVA followed by Tukey's multiple comparisons test (A and B).

and the mRNA expression of *IL-6* (Fig. 5E) and *IL-1β* (Fig. 5F). However, the increases in the production of inflammatory factors that were induced by LAMP2A deficiency were blocked by two p300 antagonists: CPI637 (Fig. 5, D to F) and A485 (fig. S4A). Moreover, knockdown of *p300* significantly repressed LPS-induced iNOS expression and abolished the effects of knockdown of *LAMP2A* (Fig. 5G), further suggesting the role of p65 acetylation by p300 in the microglial inflammatory response. In line with this, the p300 agonist CTPB abolished the inhibitory effects of CA on LPS-induced expression of iNOS (Fig. 5H). It has been reported that acetylation of p65 at lysine-218 and lysine-221 by p300 prolongs p65 nuclear localization due to its lower affinity for the negative regulator IκBα (*40*). Because we found that CMA regulated p300-mediated p65 acetylation, we wondered about the effects of CMA activation on the translocation of p65. In BV2 cells that were treated with LPS for 30 min, p65 still resided in the nucleus (Fig. 5, I to L, and fig. S4B). However, pretreatment with CA promoted the nuclear-to-cytoplasmic translocation of p65 in LPS-

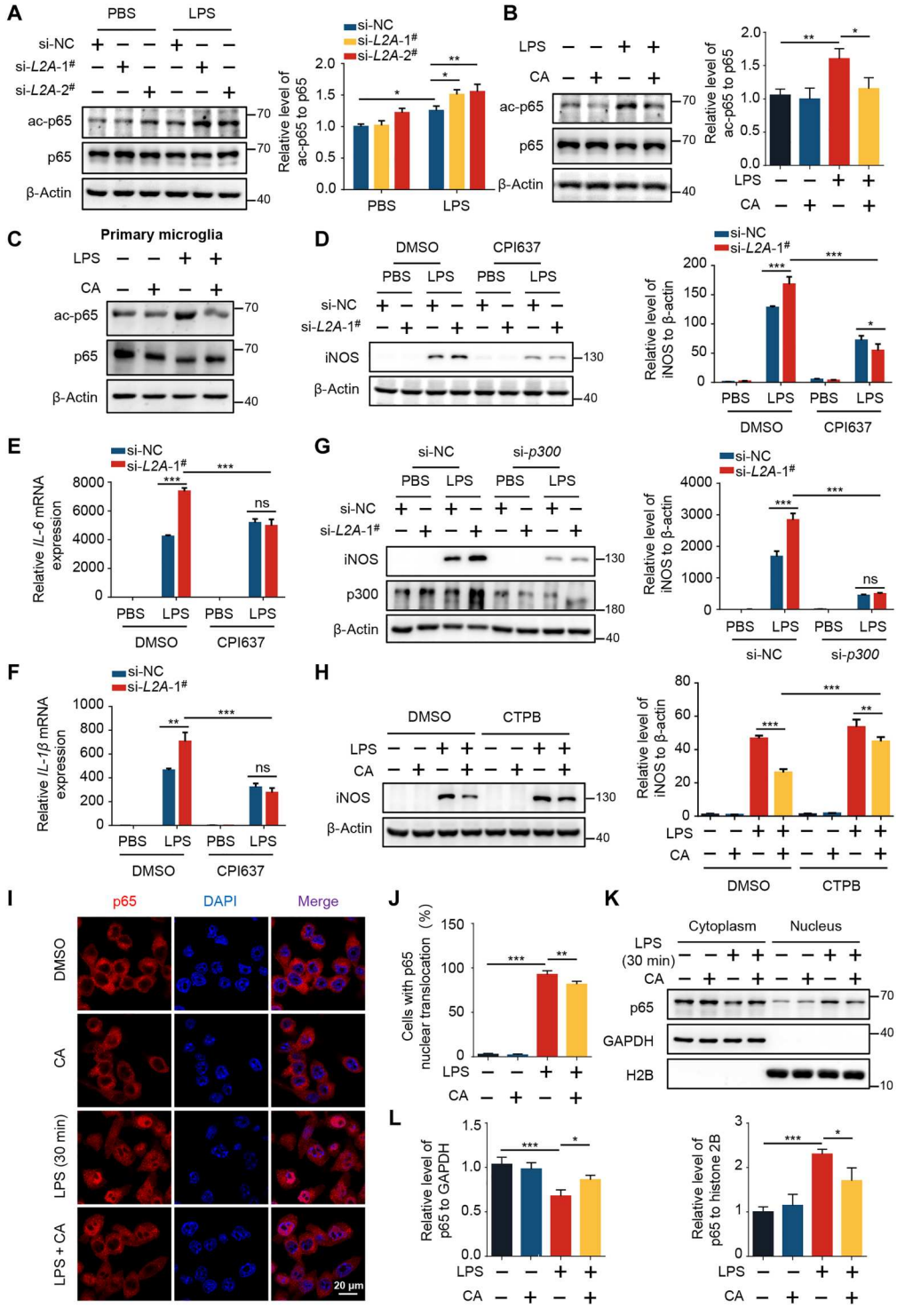

Fig. 5. p300-mediated p65 acetylation is involved in the anti-inflammatory effects of CMA activation. (**A** and **B**) Immunoblot analyses with quantification of the indicated protein levels in BV2 cells that were transfected with control siRNA or *LAMP2A* siRNAs for 48 hours (A) or pretreated with 12 μM CA for 12 hours (B) and then treated with LPS for 1 hour. $n = 3$. (**C**) Immunoblot analyses of the indicated protein levels in primary microglia that were pretreated with 20 μM CA for 24 hours and then exposed to LPS for 1 hour. (**D** to **F**) BV2 cells were transfected with control siRNA or *LAMP2A* siRNA for 36 hours, followed by treatment with 0.2 μM CPI637 for 12 hours. The cells were then exposed to LPS. Immunoblot analyses with quantification of protein levels of iNOS (D), and qPCR analyses of mRNA levels of *IL-6* (E) and *IL-1β* (F). $n = 3$. (**G** and **H**) BV2 cells were transfected with control siRNA or *LAMP2A* siRNA for 12 hours, followed by transfection with control siRNA or *p300* siRNA for 36 hours. The cells were then exposed to LPS for 16 hours (G). BV2 cells were pretreated with 12 μM CA and 20 μM p300 agonist CTPB for 12 hours and then exposed to LPS for 16 hours (H). Immunoblot analyses with quantification of protein levels of iNOS. $n = 3$. (**I** to **L**) BV2 cells were pretreated with 12 μM CA for 12 hours and then exposed to LPS for 30 min. Representative images of p65 staining (I). The cells with p65 nuclear translocation were quantified (J). Immunoblot analyses (K) with quantification (L) of protein levels of p65 in the cytoplasm and nucleus using subcellular fractionation assays. $n = 3$. One-way ANOVA followed by Dunnett's multiple comparisons test (B, J, and L) and two-way ANOVA followed by Tukey's multiple comparisons test (A and D to H).

stimulated BV2 cells that were subjected to immunofluorescence staining (Fig. 5, I and J) and fractionation assays (Fig. 5, K and L). These data indicate that p300-mediated p65 acetylation is involved in CMA-mediated regulation of inflammation.

p300 is a bona fide substrate of CMA

It is well accepted that CMA is responsible for degrading proteins and maintaining protein homeostasis (*28*, *41*). Because CMA has effects on p300-mediated p65 acetylation, we wondered whether p300 was a substrate of CMA. In 293T cells, inhibition of lysosomal activity by two chemicals, NH_4Cl and leupeptin (N/L), resulted in a remarkable increase in p300 levels in a time-dependent manner

(Fig. 6A). In addition, N/L treatment blocked CA-induced degradation of p300 (Fig. 6B). In cells that were treated with serum deprivation for CMA activation, the p300 levels were decreased (Fig. 6C), whereas N/L treatment also blocked serum deprivation-induced degradation of p300 (Fig. 6D). It has been reported that all CMA substrates must contain at least one KFERQ-like motif that is recognized by HSC70 (*17*, *18*). Sequence analysis revealed that p300 has three putative KFERQ-like motifs (Fig. 6E) (*42*). We first tested the binding ability of p300 to HSC70. Immunoprecipitation assays showed that p300 was associated with HSC70 (Fig. 6F). We next created three mutants and examined their associations with HSC70. Among the three mutants, the mutant in which Gln-Asp-Arg-Phe-Val (QDRFV) was converted to Ala-Ala-Arg-Phe-Val (AARFV) was greatly decreased in its binding to HSC70 (Fig. 6G), suggesting that this motif is responsible for the p300 interaction with HSC70. Using immunofluorescence analyses, we also observed that p300 partly colocalized with HSC70 (Fig. 6H) and LAMP2A (Fig. 6I), further suggesting p300 association with HSC70 and degradation by lysosomes.

To further confirm the degradation of p300 by CMA, we knocked down *LAMP2A* in BV2 cells. The protein levels of p300 were increased in LAMP2A-deficient BV2 cells (Fig. 6J). The activation of CMA by CA induced a time-dependent decrease in p300 (Fig. 6K). Moreover, neither *LAMP2A* siRNA (fig. S5A) nor CA (fig. S5B) treatment changed the mRNA expression of *p300* in BV2 cells. Furthermore, knockdown of *LAMP2A* significantly repressed CA-induced p300 degradation (Fig. 6L). The effects of LAMP2A on p300 degradation were further verified in BV2 cells in which *LAMP2A* was knocked out, which showed an increase in the expression of p300 (fig. S5C). In addition, CMA activation by serum deprivation induced p300 protein degradation (fig. S5D). In primary microglia, CA treatment effectively blocked LPS-induced up-regulation of p300 (Fig. 6M). Moreover, knockdown of *LAMP2A* in primary microglia increased the protein levels of p300 (Fig. 6N). In addition, p300 also partly colocalized with LAMP2A (Fig. 6O) and HSC70 (fig. S5E) in primary microglia. Thus, our data suggest that p300 is a substrate of CMA.

CMA activation inhibits microglia-mediated DA neuronal death

Increasing evidence has shown that a large number of inflammatory factors can be released by activated microglia to damage neighboring neurons (*43*). As we have found that CA inhibits microglial activation, we speculated that CA could ameliorate the neurotoxicity caused by microglial activation. To test this possibility, we cultured the DA cell line SH-SY5Y cells and primary cortical neurons with conditioned medium (CM) that were harvested from LPS-stimulated BV2 cells or primary microglia with or without CA pretreatment (Fig. 7A). SH-SY5Y cells treated with CM from LPS-treated BV2 cells exhibited increases in positive propidium iodide (PI) staining (Fig. 7, B and C). However, the toxicity of the CM from LPS-treated BV2 cells was decreased if BV2 cells were pretreated with CA, showing decreases in positive PI staining (Fig. 7, B and C) in SH-SY5Y cells. Furthermore, lactate dehydrogenase (LDH) assays (Fig. 7D), immunofluorescence staining for cleaved caspase-3 (Fig. 7, E and F), Cell Counting Kit-8 (CCK8) assays (Fig. 7G), and immunoblot analyses for cleaved caspase-3 (Fig. 7H) showed decreased cell death of SH-SY5Y cells that were exposed to CM from LPS-treated BV2 cells if they were pretreated with CA. Similar data were obtained using CM from primary microglia. Using primary neurons that were exposed to CM from microglia that were treated with LPS in combination with or without CA pretreatment, immunofluorescence staining for microtubule associated protein 2 (MAP2) revealed that the decreases in neurites in primary neurons that were exposed to CM from LPS-treated microglia were attenuated if microglia were pretreated with CA (Fig. 7, I and J). In addition, the release of LDH (Fig. 7K) in primary neurons was decreased when they were subjected to CM from microglia that were pretreated with CA. Thus, our data suggest that CMA activation attenuates microglia-mediated neurotoxicity.

CMA is dysregulated in inflammation

Because we have shown that CMA negatively regulates LPS-induced microglial activation, we wondered what happens to CMA when microglia are activated. In primary microglia after LPS treatment, LAMP2A protein decreased, and its substrate p300 protein increased (Fig. 8A). The decrease in LAMP2A protein levels should be at the transcriptional level, as the mRNA levels of *LAMP2A* were decreased after LPS treatment (Fig. 8B). Moreover, in U2OS cells treated with TNF-α, the expression of LAMP2A was decreased, while the expression of its substrate p300 was increased (Fig. 8C). In addition, immunofluorescence staining for LAMP2A also revealed that LPS stimulation reduced the expression of LAMP2A in primary microglia (Fig. 8D), further suggesting dysfunction of CMA in LPS-treated microglia.

CMA activation inhibits neuroinflammation and microglia-mediated neuronal loss in a mouse model of LPS-induced neuroinflammation

As we have shown that CMA activation has anti-inflammatory effects in vitro, we wondered whether CMA activation could alleviate neuroinflammation and promote the survival of DA neurons in vivo. Because CA has been reported to activate microglial CMA in vivo and penetrate the blood-brain barrier better than other CMA activators (*25*, *44*), we chose CA for further characterization. After intraperitoneal administration with or without CA, C57BL/6J mice received a stereotactic injection of LPS into the substantia nigra (Fig. 9A). To test the protective effects of CMA activation in vivo, we extracted protein and total RNA from mouse midbrains. We found that CA pretreatment actually activated CMA and reversed LPS-induced down-regulation of *LAMP2A* at the transcriptional level (Fig. 9B). In addition, CA pretreatment decreased the transcriptional levels of the proinflammatory factors *iNOS* (Fig. 9C), *COX-2* (Fig. 9D), *IL-6* (Fig. 9E), and *IL-1β* (Fig. 9F) that were induced by LPS injection. In mouse midbrains, LPS markedly increased the levels of ionized calcium–binding adapter molecule 1 (IBA1; microglia marker) and glial acidic fibrillary protein (GFAP; astrocyte marker) in the midbrain (Fig. 9, G and H). However, CA pretreatment decreased the expression of IBA1 and GFAP (Fig. 9, G and H) and reduced the LPS-induced loss of tyrosine hydroxylase (TH^+) neurons (Fig. 9I). In four behavioral tests, namely, the pole test, beam walking test, rotarod test, and open-field test, which evaluate the locomotor ability of each group of mice, pretreatment with CA significantly improved the locomotor capacity of LPS-stimulated mice (Fig. 9, J to N). Thus, CMA activation represses neuroinflammation and protects DA neurons in LPS-induced neuroinflammation model mice.

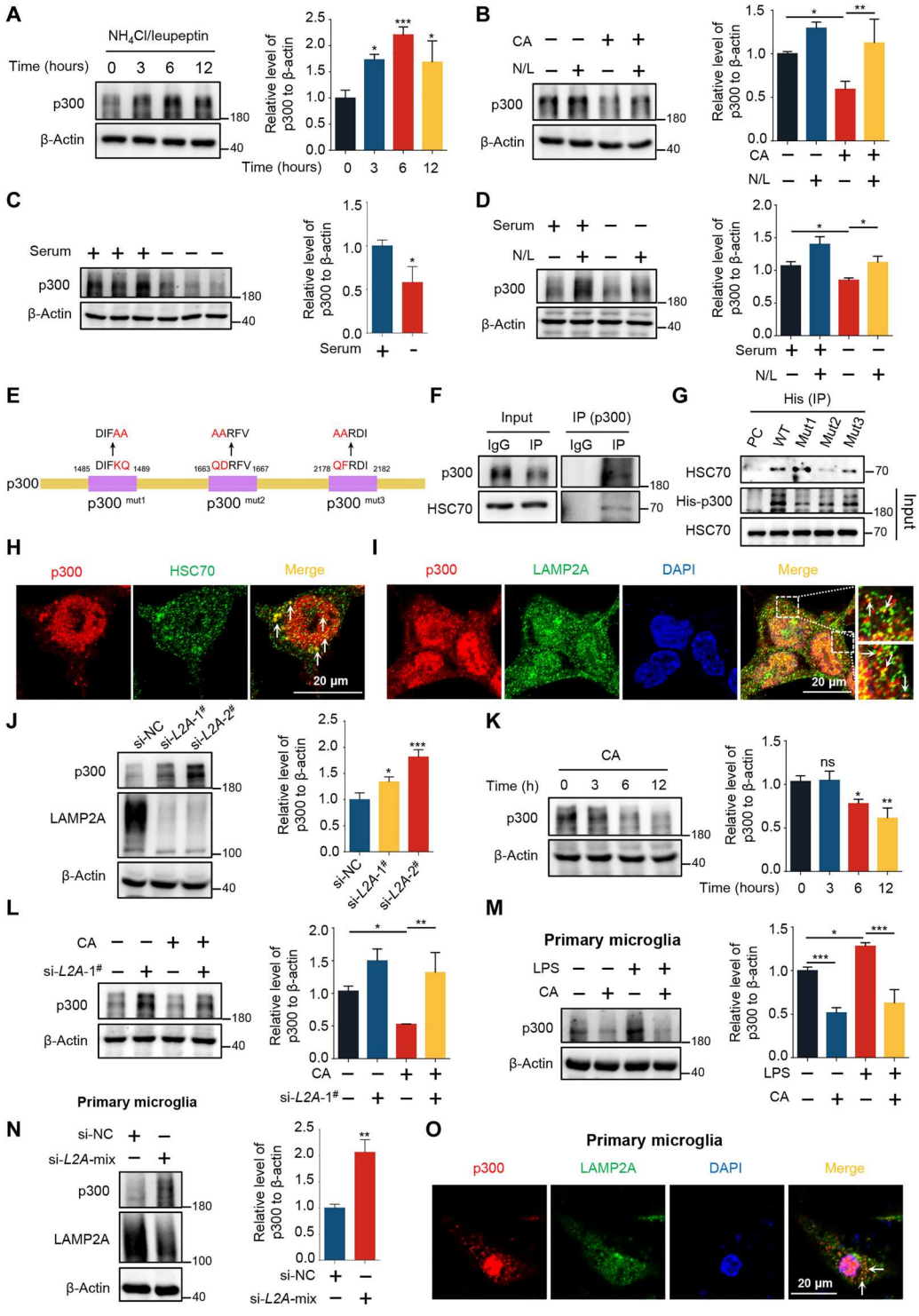

Fig. 6. p300 is a bona fide substrate of CMA. (**A** to **D**) 293T cells were treated with 10 mM NH_4Cl and 50 μM leupeptin (N/L) (A). 293T cells were pretreated with 20 μM CA for 6 hours and then exposed to N/L for 6 hours (B). 293T cells were cultured with or without serum for 24 hours (C). 293T cells were precultured with or without serum for 12 hours and then exposed to N/L or not for 12 hours (D). Immunoblot analyses with quantification of protein levels of p300. $n = 3$. (**E**) Schematic diagram of three p300 mutants. (**F** and **G**) The supernatants of 293T cell lysates were subjected to immunoprecipitation with anti-p300 antibodies or normal mouse immunoglobulin G (IgG) (F). The supernatants from the cell lysates of 293T cells that were transfected with His-pcDNA3.1, wild-type p300 plasmid, and three p300 mutants were subjected to immunoprecipitation with His-Tag Purification Resin (G). Immunoblot analyses of the indicated protein levels. IP, immunoprecipitation. (**H** and **I**) Representative images of p300, HSC70, and LAMP2A staining in 293T cells. (**J** to **L**) Immunoblot analyses with quantification of protein levels of p300 in 293T cells that were transfected with control siRNA or *LAMP2A* siRNAs for 48 hours (J) and then treated with 12 μM CA for 12 hours (L) or treated with 12 μM CA for indicated time (K). $n = 3$. (**M** and **N**) Immunoblot analyses with quantification of protein levels of p300 in primary microglia that were pretreated with 20 μM CA for 24 hours and then exposed to LPS for 16 hours (M) or transfected with control siRNA or *LAMP2A* siRNA-mix for 48 hours (N). $n = 3$. (**O**) Representative images of p300 and LAMP2A staining in primary microglia. Unpaired *t* test (C and N), one-way ANOVA followed by Dunnett's multiple comparisons test (A, B, D, and J to L), and two-way ANOVA followed by Tukey's multiple comparisons test (M).

DISCUSSION

Microglia are resident myeloid macrophages in the central nervous system that serve as immunological surveillants and maintain brain homeostasis (*43*). During the pathological progression of PD, microglia change into a proinflammatory state, resulting in inflammatory damage to neighboring DA neurons. It has been reported that CMA is associated with inflammation-related diseases, including PD. CMA degrades oxidized myocyte enhancer factor 2D (MEF2D) and oxidized/nonfunctional DJ-1, thereby contributing to the survival of DA neurons (*28*, *41*). In addition, both mutant α-synuclein and dopamine-modified α-synuclein and $LRRK2^{G2019S}$ or $LRRK2^{R1441G}$ mutants reduce the activity of CMA by binding to LAMP2A (*24*, *27*, *45*, *46*). In activated T cells, CMA degrades itchy E3 ubiquitin protein ligase (ITCH), an

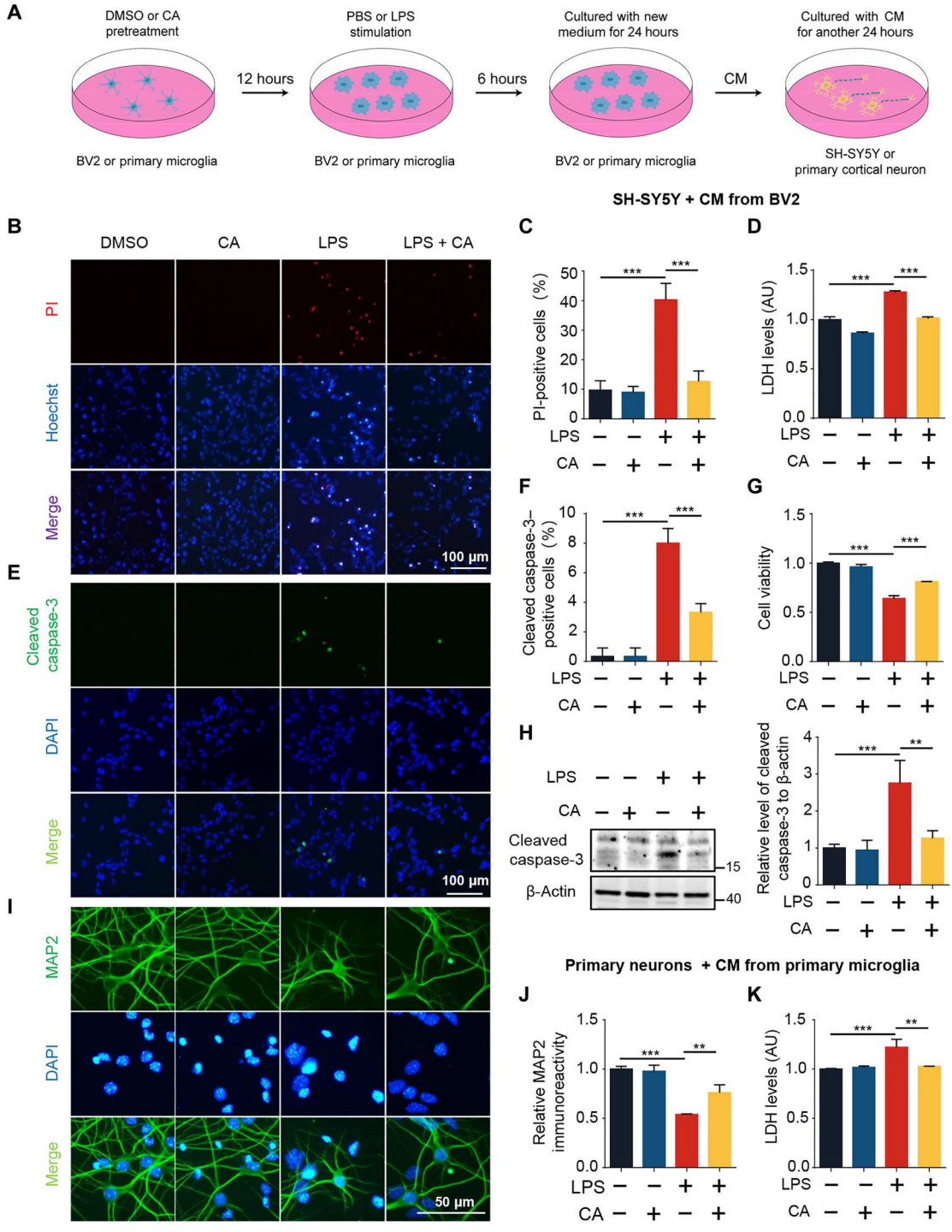

Fig. 7. CMA activation inhibits microglia-mediated DA neuronal death. (**A**) A schematic diagram of the conditioned medium (CM) assay. (**B** to **H**) SH-SY5Y cells were cultured with CM from BV2 cells for 24 hours. Representative images of propidium iodide (PI) staining in SH-SY5Y cells (B). The PI-positive cells were counted and quantified with cell numbers marked with Hoechst (C). LDH was detected to indicate cell death (D). AU, arbitrary units. Representative images of cleaved caspase-3 staining in SH-SY5Y cells (E). The cleaved caspase-3–positive cells were counted and quantified with cell numbers marked with 4′,6-diamidino-2-phenylindole (DAPI) (F). CCK8 was detected to indicate cell viability (G). Immunoblot analyses with quantification of protein levels of cleaved caspase-3 (H). $n = 3$. (**I** to **K**) Primary cortical neurons were cultured with CM from primary microglia for 24 hours. Representative images of MAP2 staining in primary cortical neurons (I). The relative fluorescence intensity of MAP2 was quantified (J). Cell death was indicated by LDH assays (K). $n = 3$. One-way ANOVA followed by Dunnett's multiple comparisons test (C, D, F to H, J, and K).

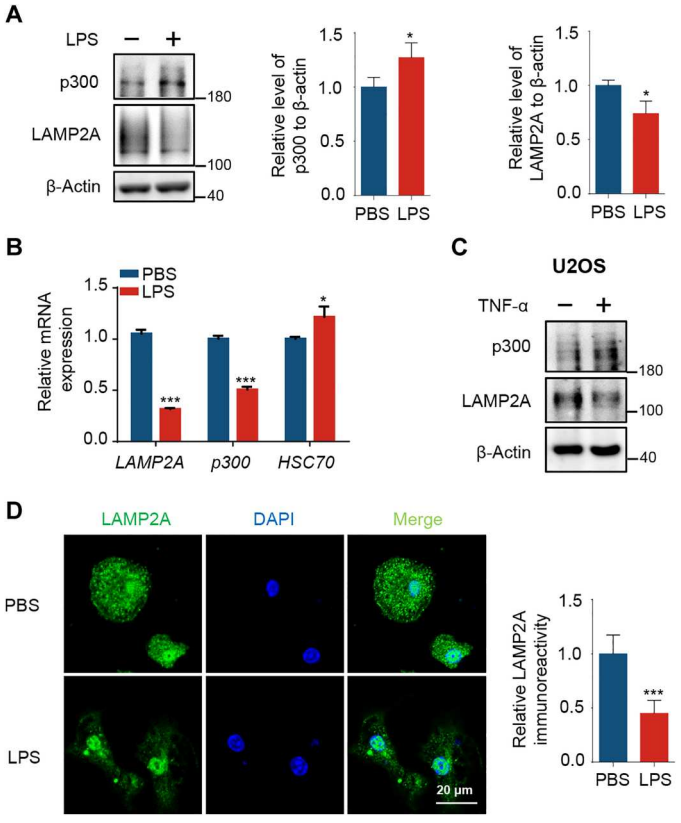

Fig. 8. CMA is dysregulated in inflammation. (**A** and **B**) Immunoblot analyses with quantification of protein levels of p300 and LAMP2A (A), and qPCR analyses of mRNA levels of *LAMP2A*, *p300*, and *Hsc70* (B) in primary microglia that were treated with LPS for 24 hours. $n = 3$. (**C**) U2OS cells were treated with TNF-α (20 ng/ml) for 24 hours. The protein levels of p300 and LAMP2A were measured using immunoblot analyses. (**D**) Representative images of LAMP2A staining in primary microglia that were treated as described in (A). The relative fluorescence intensity of LAMP2A was quantified. $n = 12$. Unpaired *t* test (A, B, and D).

ubiquitin ligase, and regulator of calcineurin 1 (RCAN1), a calcineurin inhibitor, to maintain the T cell response (*47*). Moreover, CMA targets NLRP3 for lysosomal degradation to suppress the activation of the NLRP3 inflammasome in macrophages and microglia (*48*, *49*). The accumulation of Nup85 caused by CMA blockade aggravates inflammation in macrophages (*50*). Our current study demonstrates that CMA dysfunction promotes LPS-induced microglial activation, whereas CMA activation represses microglia-mediated neuroinflammation. We show that microglial CMA activation represses microglial activation and protects DA neurons from inflammatory cell death in vitro and in vivo.

Under LPS stimulation, activation of TLR4 recruits myeloid differentiation factor 88 (MyD88)/MyD88-adapter-like (MAL) and TIR domain-containing adaptor inducing interferon-β (TRIF)/TRIF-related adaptor molecule (TRAM) to phosphorylate transforming growth factor β-activated kinase 1 (TAK1), which, in turn, activates the NF-κB and AP-1 signaling pathways to trigger an inflammatory response (*51*). In our study, we demonstrate that the NF-κB pathway, but not AP-1, is involved in the CMA-mediated repressive effects on LPS-induced inflammation in microglia. NF-κB activation is typically characterized by the nuclear translocation of p65. It has been reported that inhibition of CMA in mesenchymal stromal cells enhances the expression of C-X-C motif chemokine 10 (CXCL10) and iNOS by activating NF-κB and signal transducer and activator of transcription 1 (*52*). In addition, p65 is a substrate of CMA (*53*), further suggesting a link between CMA and NF-κB. In our study, we found that CMA negatively regulates LPS-induced NF-κB transcriptional activity through the acetylation of NF-κB by p300, although CMA activation does not influence p65 expression or phosphorylation.

The transcriptional activity of p65 in the nucleus is regulated by multiple posttranslational modifications, such as phosphorylation and acetylation (*54*–*56*). The histone acetyltransferases p300, CREB-binding protein (CBP), and p300/CBP-associated factor (PCAF) and the histone deacetylases HDAC1 and HDAC2 are responsible for the acetylation of p65 (*56*). In addition, two p300 antagonists, A485 and C646, can attenuate LPS-mediated macrophage activation by reducing NF-κB activity (*38*, *57*), indicating that p300-mediated p65 acetylation is important for NF-κB–mediated inflammation. Using *p300* siRNA, p300 antagonists, and a p300 agonist, we identified that CMA affects NF-κB activation through p300-mediated p65 acetylation, thereby regulating the LPS-induced production of proinflammatory factors. Although in CA-treated cells, the phosphorylation and nuclear translocation of NF-κB remained unchanged 10 min after LPS treatment, CA-induced degradation of p300 by CMA decreased NF-κB acetylation and led to a shorter retention of NF-κB in the nucleus, which attenuated NF-κB–mediated inflammation.

In our study, we identified p300 as a substrate of CMA. CMA substrates contain at least one KFERQ-like motif (*18*). It has been reported that p300 protein levels were significantly elevated in LAMP2A-deficient SN4741 cells from mass spectrometry screening data (*32*) and that 5-fluorouracil promotes CMA-dependent p300/CBP degradation, thereby inhibiting the progression of colorectal cancer (*58*), suggesting that p300 is a potential substrate of CMA. Here, we further show that p300 interacts with the CMA chaperone HSC70 and the CMA-limiting protein LAMP2A. A conversion of QDRFV, the second predicted KFERQ-like motif that is recognized by HSC70, to AARFV abolishes the interactions between p300 and HSC70. In addition, LAMP2A deficiency induces an increase in p300 levels. As HSC70 is responsible for substrate recognition and LAMP2A for substrate transport to lysosomes, our data suggest that p300 is a substrate of CMA. Although p300 is mainly located in the nucleus, it can be phosphorylated by mechanistic target of rapamycin complex 1 (mTORC1) on lysosomes and detected in purified lysosomes (*59*). Furthermore, we demonstrate that inhibition of lysosomal activity by N/L increases p300 protein levels, suggesting that p300 can be degraded by lysosomes, similar to other nuclear proteins, such as checkpoint kinase 1 and p21 (*60*, *61*).

Upon LPS treatment, the expression of LAMP2A was significantly decreased in primary microglia, while the protein levels of p300 were increased. Unexpectedly, the mRNA levels of p300 were decreased, so we speculated that the decrease may be a compensatory effect or a regulatory result of other pathways. Our data provide a mechanistic link among NF-κB–mediated inflammation, LAMP2A-driven CMA, and p300-related acetylation. CMA-mediated degradation of p300 has repressive effects on microglial activation. Furthermore, CMA activation by the activator CA attenuates the activation of microglia and inflammatory damage to DA

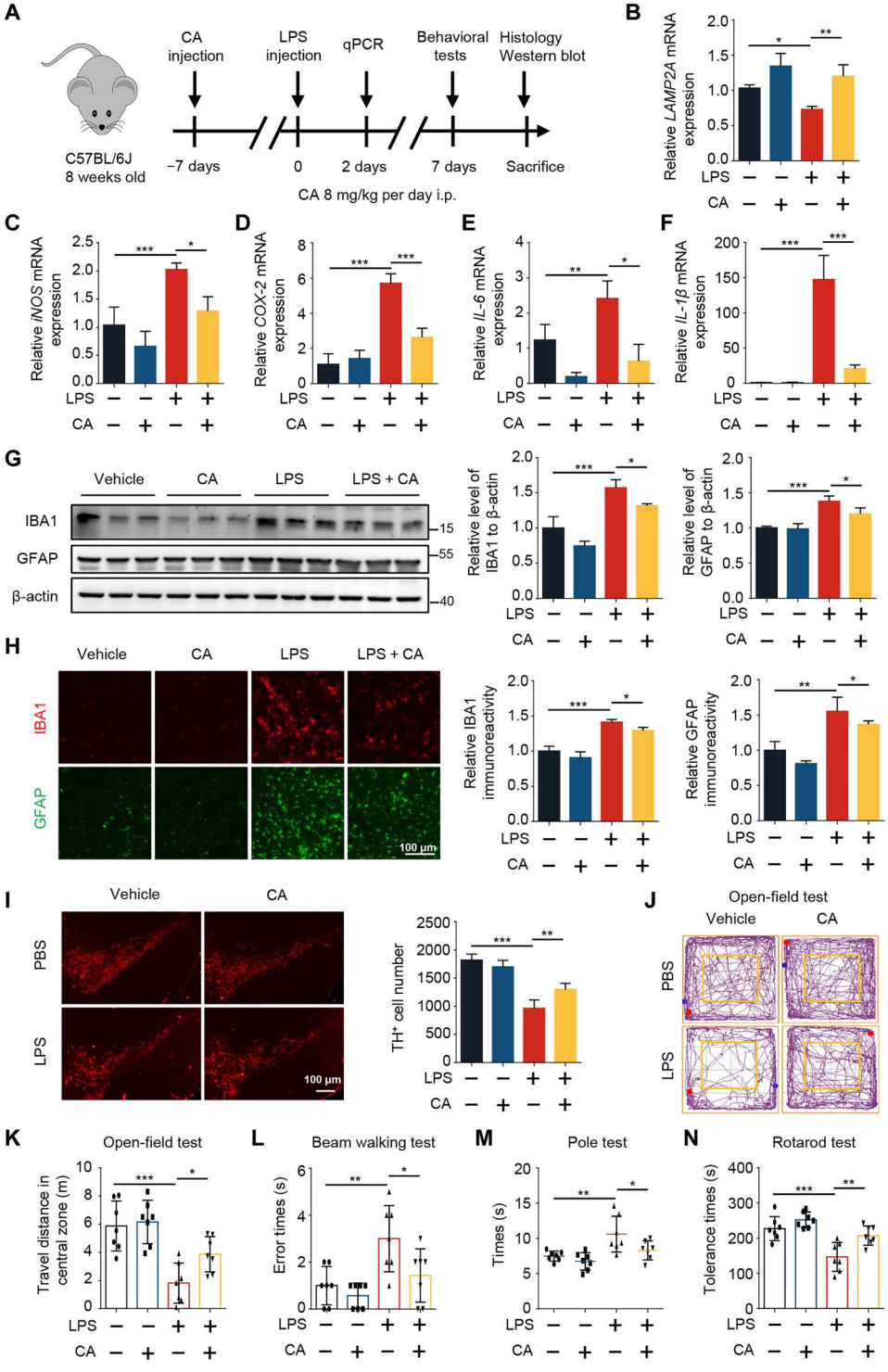

Fig. 9. CMA activation inhibits neuroinflammation and microglia-mediated neuronal loss in a mouse model of LPS-induced neuroinflammation. (**A**) A schematic diagram of the animal experimental procedure. i.p., intraperitoneal. (**B** to **F**) qPCR analyses of mRNA levels of *LAMP2A* (B), *iNOS* (C), *COX-2* (D), *IL-6* (E), and *IL-1β* (F) in the midbrains isolated from different groups. $n = 3$. (**G**) Immunoblot analyses with quantification of protein levels of ionized calcium–binding adapter molecule 1 (IBA1) and glial acidic fibrillary protein (GFAP) in the midbrains isolated from different groups. $n = 3$. (**H** and **I**) Representative images of IBA1 (H), GFAP (H), and TH (I) staining in the midbrains isolated from different groups. The relative fluorescence intensities of IBA1 and GFAP were quantified (H). $n = 4$. The cell number of TH^+ cells was also quantified (I). $n = 5$. (**J** to **N**) Behavioral tests were conducted. $n = 7$. Representative images of the movement paths of the four mouse groups monitored for 15 min (J). The travel distance in the central area of the open field (K). The number of foot slips in the beam walking test (L). The climbing time in the pole test (M). The latencies to fall from the accelerated rotating beams in the rotarod test (N). One-way ANOVA followed by Dunnett's multiple comparisons test (B to N).

neurons in vitro and in vivo and improves motor abilities in LPS mice, reflecting that CMA-related microglial regulation plays important roles in PD pathogenesis. However, there are still some limitations that need to be considered in our study. First, in CA-treated LPS mice, we cannot exclude the possibility that CMA activation by CA may protect neurons by decreasing the astrocyte response to microglial activation and increasing neuronal resistance to cytokines produced by activated microglia. Second, we explore the effects and mechanisms of CMA on microglial activation in BV2 microglial cell line, whose LPS reactivity and expression profile are not identical to those of primary microglia in vitro or in vivo (*62*). It has been reported that down-regulation of neuronal LAMP2A by adeno-associated virus (AAV)–mediated delivery of short hairpin RNAs leads to the accumulation of α-synuclein and the loss of DA neurons (*63*). Their data suggest that a half decrease in LAMP2A levels in neurons by AAV-mediated knockdown induces phenotypes in animals (*63*). Together with our data, it suggests that loss of half of LAMP2A sufficiently induces dysfunction of CMA in both neurons and microglia (*63*). The microglia-specific *LAMP2A* conditional KO mice should be of help to address this issue in the future work. Recently, CA was reported to improve amyloid-β deposition in two different animal models of AD and protect against retinal degeneration by activating CMA (*25*, *44*). Thus, CMA is functionally associated with inflammation and neurodegenerative diseases. It is of help to develop specific activators targeting CMA, which may have greater potential to repress neuroinflammation and protect neurons.

In summary, our study provides a mechanistic explanation of CMA in microglial activation (Fig. 10). CMA negatively regulates microglia-mediated neuroinflammation. The activation of CMA promotes the degradation of the CMA substrate p300, which reduces p300-mediated p65 acetylation, leading to a decrease in NF-κB activity and, in turn, inhibiting NLRP3 inflammasome activation and the release of proinflammatory factors. The activation of CMA effectively represses microglial activation and protects DA neurons from inflammatory damage. Thus, CMA activation has potential as a therapeutic tool for the treatment of neurodegenerative diseases.

MATERIALS AND METHODS

Experimental animals

Male C57BL/6J mice (age 6 to 8 weeks, 20 to 25 g) were purchased from Shanghai Laboratory Animal (Shanghai, China). All animals were raised in a 12-hour light/dark cycle with free access to food and water. All animal experiments performed in this study were in accordance with the institutional guidelines for the use and care of animals, and all procedures were approved by the Institute Animal Welfare Committee of Soochow University. For LPS treatment, all animals were randomly divided into four groups: (i) vehicle + phosphate-buffered saline (PBS) group, (ii) CA + PBS group, (iii) vehicle + LPS group, and (iv) CA + LPS group. Mice in groups (ii) and (iv) were intraperitoneally injected with CA (8 mg/kg per day) for seven consecutive days. CA (HY-134923) was purchased from MedChemExpress (Monmouth Junction, NJ, USA). Meanwhile, the mice in the other groups were administered an equal volume of vehicle. The vehicle contained 45% polyethylene glycol 300, 5% Tween 80, and 50% normal saline. On day 6, the bilateral SNpc of each mouse mentioned above was treated with LPS (2 μg) or an equal volume of PBS using stereotaxic injection at anterior-posterior of −3.3 mm, medial-lateral of ±1.2 mm, and dorsal-ventral of −4.6 mm from bregma. All animals were treated with CA or vehicle for another 7 days. After behavioral experiments, the animals were euthanized, and the brain tissues were harvested for further analysis.

Behavioral experiments

Four animal behavioral tests, namely, the beam walking test, pole test, rotarod test, and open-field test, were performed to assess fine motor skills and balance. The behavioral instruments were purchased from SANS Biological Technology (Nanjing, China). The testing room was kept quiet, and the spontaneous activity of the mice was maintained. The animal training and experimental methods are relevant to previous studies (*35*, *64*).

For beam walking test, the apparatus consists of a 50 cm–by–5 cm (length by width) beam that is 50 cm above the floor and a dark box (10 cm by 10 cm by 10 cm) at the end of the beam. On the day of training, each mouse was trained to cross the beam into the dark box without pausing. On the day of testing, the number of hindlimb slips of each mouse was counted. The experiment was repeated three times for each mouse, and the average times were analyzed.

For pole test, on the day of training, each mouse was placed on the top of a wood pole (50 cm in height and1 cm in diameter) in the home cage and then allowed to climb into the cage for three times. On the day of testing, the time required for each mouse to climb into the cage was recorded. The experiment was repeated three times for each mouse, and the average times were analyzed.

For rotarod test, on the day of training, each mouse was placed on the rotarod until it was able to stay on the rotarod for at least 5 min at a speed of 4 rpm. On the day of testing, for each mouse, the latency time to fall was recorded when the rotarod speed was accelerated from 4 to 40 rpm in 5 min. The experiment was repeated three times for each mouse.

For open-field test, a 40 cm–by–40 cm by–40 cm square arena is divided into 16 equal squares, of which the central four squares define the central area. After each mouse was placed in the corner of the square arena, it was allowed to crawl freely for 15 min while being recorded on video. The travel distance in the center area of each mouse was analyzed.

Cell culture and drug treatment

BV2 cells, a murine microglial cell line, were incubated in Dulbecco's modified Eagle's medium (DMEM) (Gibco, Grand Island, NY, USA) with 10% heat-inactivated fetal bovine serum (FBS), penicillin (100 μg/ml), and streptomycin (100 μg/ml). SH-SY5Y cells, a DA cell line, were cultured in DMEM/F12 with 10% FBS, penicillin (100 μg/ml), and streptomycin (100 μg/ml). Human embryonic kidney 293T (HEK293T) cells [CRL-3216, American Type Culture Collection (ATCC)] and HEK293T/17 cells (CRL-11268, ATCC) were cultured in DMEM with 10% FBS, penicillin (100 μg/ml), and streptomycin (100 μg/ml). Human bone osteosarcoma epithelial cells (U2OS) were cultured in DMEM with 10% FBS, penicillin (100 μg/ml), streptomycin (100 μg/ml), and 1 M Hepes. Primary cultured microglia were isolated from 3-day-old C57BL/6J mice, and primary cortical neurons were dissociated from the cortex of C57BL/6J mouse embryos at embryonic day 17. These two types of primary cultured cells were obtained and cultured as described previously (*35*, *65*). CA (S6395) used for cells was

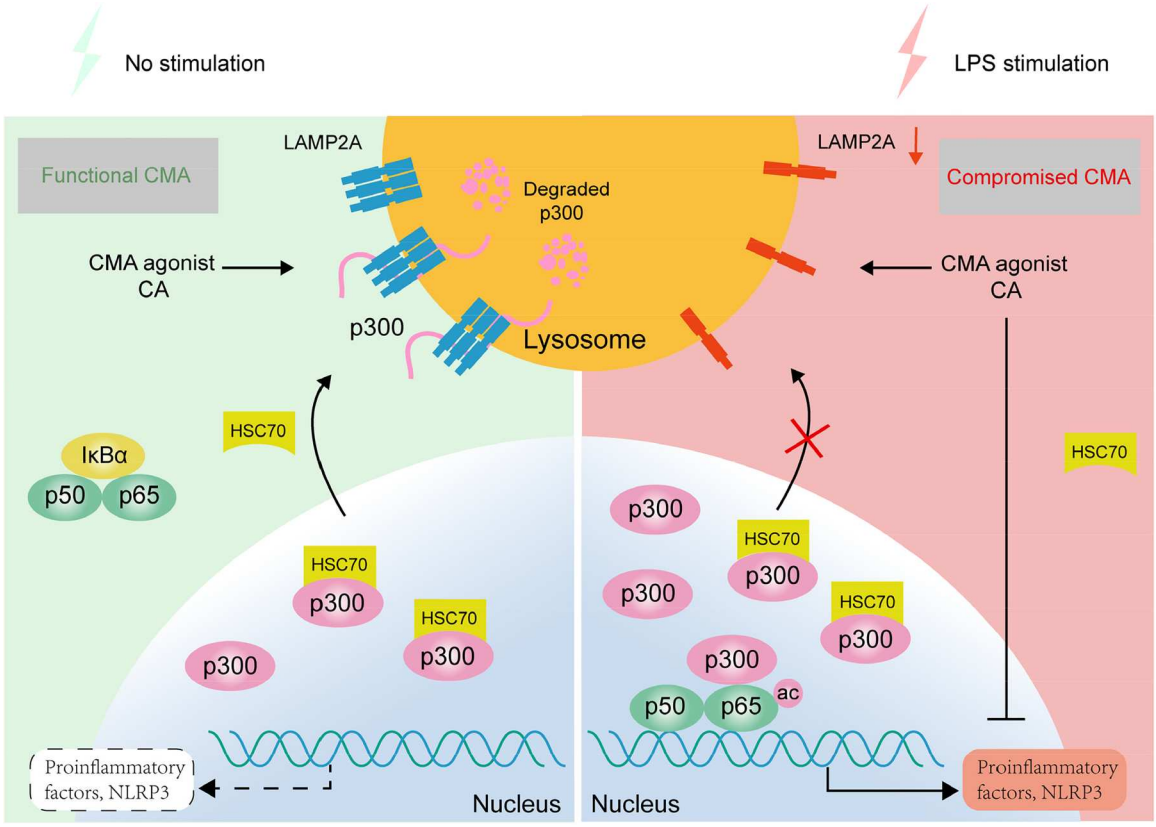

Fig. 10. A schematic diagram shows that CMA is involved in the microglial inflammatory response. Under normal conditions, p300 is recognized by HSC70 and then transferred to lysosomes for degradation, which is mediated by LAMP2A-driven CMA, and the CMA activator CA accelerates this process. However, upon LPS stimulation, LAMP2A is markedly decreased, leading to the accumulation of p300 in the nucleus, which promotes p65 acetylation. The acetylation of p65 leads to the retention of NF-κB in the nucleus and increases the transcriptional activity of NF-κB, which subsequently promotes the activation of the NLRP3 inflammasome and the production of proinflammatory factors, aggravating DA neuronal death, which can be alleviated by CA.

purchased from Selleck Technology (Houston, TX, USA). QX77 (HY-112483), IMD0354 (HY-10172), CPI637 (HY-100482), A485 (HY-107455), TNF-α (HY-P70426A), and LPS (HY-D1056) were purchased from MedChemExpress. All were dissolved in dimethyl sulfoxide except LPS and TNF-α, which were dissolved in PBS. The concentration of LPS used for cells was 1 μg/ml.

RNA interference

LAMP2A and *p300* siRNAs were purchased from GenePharma (Shanghai, China) with the following sequences as described previously: si-NC sense: 5′-AUGGCAUCAUAAGCUGCACAC-3′; si-*LAMP2A*-1$^{\#}$: 5′-GGUCUCAAGCGCCAUCAUATT-3′; si-*LAMP2A*-2$^{\#}$: 5′-CTGCAATCTGATTGATTA-3′ (*66*); and si-*p300*: 5′-UAUUUAUCAAACUUAAUCCAG-3′. Lipofectamine RNAiMAX Transfection Reagent (Invitrogen, Carlsbad, CA, USA) was used to transfect siRNAs into BV2 cells and primary microglia according to the manufacturer's instructions. For instance, we first transfected BV2 cells with 80 nM si-*LAMP2A*-1$^{\#}$ or 80 nM si-*LAMP2A*-2$^{\#}$ for 24 hours, whereas a mixture of 24 nM si-*LAMP2A*-1$^{\#}$ and 24 nM si-*LAMP2A*-2$^{\#}$ (called si-*LAMP2A*-mix) was used in primary microglia. Next, the medium was replaced with fresh medium. One day later, the cells were treated with LPS or PBS for 16 hours and then harvested for further assays.

Plasmid transfection

The p300-pcDNA3.1 plasmid (no. 74658, Addgene, USA) was a gift from L. Zheng (Soochow University, Suzhou, China). Three mutants of p300 were constructed by GENEWIZ (Suzhou, China). 293T cells were seeded in 24-well plates and then transfected with wild-type or mutant p300 plasmids using Lipofectamine 2000 reagent (Invitrogen) for 48 hours. The cells were collected for further immunoprecipitation assays.

CRISPR-Cas9 KO cells

The lentiCRISPR v2 plasmid (VT8107) was purchased from Youbio (Hunan, China). The sequence of sg-*LAMP2A* was described previously (*67*): sense: CACCGAGAGCTGCTCCCACCGCTAT: and anti-sense: AAACATAGCGGTGGGAGCAGCTCTC. To generate *LAMP2A* CRISPR KO BV2 cells, *LAMP2A* sgRNA was cloned into the lentiCRISPR v2 vector. The virus particles were produced by transient transfection into HEK293T/17 cells with lentiCRISPR v2 vectors, together with the packaging constructs and the constructs that express the vesicular stomatitis virus glycoprotein using Lipofectamine 2000 reagent. After 48 hours, lentivirus particles in the medium were collected and filtered to culture BV2 cells. After 14 days of post-puromycin (2 μg/ml) selection, surviving KO cells were verified by immunoblotting.

Cell viability assay

Cell viability was measured by a CCK8 (APExBIO Technology LLC, Houston, USA) according to the manufacturer's instructions. Briefly, BV2 cells were pretreated with CA, QX77, or siRNAs against *LAMP2A*, followed by LPS treatment. Then, the cells were incubated with 10% CCK8 reagent at 37°C for 2 hours. The absorbance was detected at 450 nm by a microplate reader to determine cell viability.

Cell cytotoxicity assay

The cytotoxicity of LDH release was detected by the CytoTox 96 Non-Radioactive Cytotoxicity Assay (Promega, Madison, WI, USA). In brief, 50 μl of growth medium collected from SH-SY5Y cells after CM incubation for 24 hours was mixed with 50 μl of CellTiter-Go and shaken for 20 min at room temperature. The absorbance was detected at 490 nm by a microplate reader to determine cell cytotoxicity.

ELISA assay and NO measurement

BV2 cells or primary microglia were plated into 24-well plates and then treated with CA, QX77, or siRNAs against *LAMP2A*, followed by LPS treatment for 24 hours. Next, 100 μl of cultured medium was detected using ELISA kits (BOSTER, Wuhan, China). After BV2 cells or primary microglia were treated in the same manner as the ELISA method, the NO concentration was measured using the Griess method with an NO assay kit (Beyotime Biotechnology, Shanghai, China) according to the manufacturer's instructions.

Quantitative real-time PCR

BV2 cells were plated into 24-well plates and then treated with CA, QX77, or siRNAs against *LAMP2A*, followed by LPS treatment for 12 hours. Next, total RNA was extracted using a TRIzol commercial kit (Invitrogen) according to the protocol described previously (*35*). Then, RNA was reverse-transcribed into cDNA with Hiscript II Q RT SuperMix (Vazyme Biotech, Nanjing, China). Real-time quantitative polymerase chain reaction (PCR) was performed using the SYBR Green PCR Master Mix (Vazyme Biotech) on an ABI 7500 PCR instrument (Applied Biosystems). The sequences of PCR primers were as follows: mouse *β-actin* sense: 5′-GACCTGACTG ACTACCTC-3′ and 5′-GACAGCGAGGCCAGGATG-3′; mouse *iNOS* sense: 5′-TCCCAGCCTGCCCCTTCAAT-3′ and 5′-CGGAT CTCTCTCCTCCTGGG-3′; mouse *COX-2* sense: 5′-CAGGCTGA ACTTCGAAACA-3′ and 5′-GCTCACGAGGCCACT GATACCTA-3′; mouse *IL-6* sense: 5′-GCTATGAAGTTCCTCTC TGC-3′ and 5′-CTAGGTTTGCCGAGTAGATC-3′; mouse *IL-1β* sense: 5′-TGGCAACTGTTCCTG-3′ and 5′-GGAAGCAGCCCTT CATCTTT-3′; mouse *LAMP2A* sense: 5′-GCAGTGCAGATGAA GACAAC-3′ and 5′-AGTATGATGGCGCTTGAGAC-3′; mouse *LAMP2B* sense: 5′-GGTGCTGGTCTTTCAGGCTTGATT-3′ and 5′-ACCACCCAATCTAAGAGCAGGACT-3′; mouse *LAMP2C* sense: 5′-ATGTGCTGCTGACTCTGACCTCAA-3′ and 5′-TGGA AGCACGAGACTGGCTTGATT-3′; mouse *NLRP3* sense: 5′-ATTACCCGCCCGAGAAAGG-3′ and 5′-TCGCAGCAAAGAT CCACACAG-3′; mouse *IL-18* sense: 5′-GACTCTTGCGTCAACTT CAAGG-3′ and 5′-CAGGCTGTCTTTTGTCAACGA-3′; mouse *p300* sense: 5′-TTCAGCCAAGCGGCCTAAA-3′ and 5′-CGCCAC CATTGGTTAGTCCC-3′; and mouse *HSC70* sense: 5′-TCTCGG CACCACCTACTCC-3′ and 5′-CTACGCCCGATCAGACGTTT-3′. The relative mRNA levels of these genes to *β-actin* were calculated using the $2^{-\Delta\Delta CT}$ method.

Immunoblot analysis and antibodies

BV2 cells or primary microglia were plated into 24-well plates and then treated with CA, QX77, or siRNAs against *LAMP2A*, followed by LPS treatment for 16 hours. Next, the cells were lysed in cell lysis buffer [0.5% deoxycholate, 1% NP-40, 50 mM tris-HCl (pH 7.5), 150 mM NaCl, and protease inhibitor cocktail (Roche)]. The isolated brain samples were first homogenized by a PRO200 homogenizer and then lysed in cell lysis buffer. Approximately 20 μg of each protein sample was separated by SDS–polyacrylamide gel electrophoresis and then transferred onto polyvinylidene difluoride membranes (EMD Millipore). Immunoblot analyses were performed with the following primary antibodies: anti-LAMP2A (51-2200) (Thermo Fisher Scientific, Waltham, MA, USA); anti-KAT3B/p300 (ab259330), anti–COX-2 (ab15191), anti–histone 2B (H2B; ab45695), anti-IκBα (ab32518), and anti–NF-κB p65 (acetyl K310) (ab19870) (Abcam, Cambridge, MA, USA); anti-iNOS (13120S), anti–NF-κB/p65 (8242S), anti–phospho–NF-κB p65 (Ser^{536}) (3033S), anti-SAPK/JNK (9252S), anti–phospho-SAPK/JNK (Thr$^{183/185}$) (4668S), anti–cleaved caspase-3 (9661S), and anti–His-Tag (12698S) (Cell Signaling Technology, Danvers, MA, USA); anti–phospho-Erk1/2 (sc-101760), anti-ERK1 (sc-271269), anti-p38 (sc-81621), anti–phospho-p38 (sc-166182), anti-HSC70 (sc-7298), anti–caspase-1 (sc-392736), and anti–β-actin (sc-8432) (Santa Cruz Biotechnology, Santa Cruz, CA, USA); anti–glyceraldehyde-3-phosphate dehydrogenase (GAPDH) (CB1001) and anti-GFAP (MAB360) (Millipore, Billerica, MA, USA); anti-NLRP3 (19771-1-AP) (Proteintech, Wuhan, China); and anti-IBA1 (019-19741) (Wako Chemicals, Tokyo, Japan). The membranes were incubated with the indicated primary antibodies for at least 12 hours and then incubated with goat anti-mouse or anti-rabbit immunoglobulin G–horseradish peroxidase secondary antibodies (Thermo Fisher Scientific, Waltham, MA, USA) for 2 hours. The proteins were eventually visualized using an enhanced chemiluminescence detection kit (Thermo Fisher Scientific).

Subcellular fractionation assay

BV2 cells were pretreated with CA for 12 hours, followed by LPS treatment for 10 or 30 min. Then, the cells were lysed in fractionation buffer containing 3 mM $CaCl_2$, 2 mM MgAc, 320 mM sucrose, 0.1 mM EDTA, 1 mM dithiothreitol, 0.5 mM phenylmethylsulfonyl fluoride, and 0.5% NP-40 for 20 min on ice. After centrifugation for 15 min at 600*g* at 4°C, the supernatants were collected as the cytoplasmic fraction. The remaining pellets, which served as the nuclear fraction, were washed twice using the fractionation buffer without NP-40 and then lysed in the cell lysis buffer described in immunoblot. H2B served as a nuclear marker, and GAPDH served as a cytoplasmic marker.

Immunoprecipitation assay

293T cells were lysed in the cell lysis buffer used for immunoblotting on ice, and, then, the cells were sonicated and centrifuged to collect supernatants. The supernatants were incubated with His-Tag Purification Resin (Beyotime Biotechnology) or Protein G Agarose (Thermo Fisher Scientific) coupled with p300 antibody (sc-48343) (Santa Cruz Biotechnology, Santa Cruz, CA, USA) overnight at 4°C. The protein complexes coupled to His-Tag

Purification Resin or Protein G Agarose were washed three times with lysis buffer. The immunoprecipitants and the input, which was 10% of the total cell lysates, were analyzed using western blotting.

Luciferase reporter gene assay

BV2 cells were transfected with the Cignal lentiviral NF-κB reporter (QIAGEN, Hilden, Japan) for 24 hours, and, then, puromycin (2 μg/ml) was used to obtain a BV2 cell line stably expressing the NF-κB reporter element. This cell line was pretreated with CA or siRNAs against *LAMP2A*, followed by LPS stimulation for 16 hours. After LPS stimulation, the cells were collected to detect NF-κB promoter activity with a luciferase assay kit (Promega, Madison, WI, USA) according to the manufacturer′s recommendations.

Immunofluorescence staining

BV2 cells, 293T cells, SH-SY5Y cells, primary neurons, or primary microglia were fixed with 4% paraformaldehyde (PFA) for 10 min and permeabilized with 0.1% Triton X-100 for another 10 min. After washing three times with PBS, 2% FBS in PBS was used to block the cells for 10 min. Next, the cells were incubated with anti–NF-κB/p65 (8242S), anti-ASC (67824S), and anti–cleaved caspase-3 (9661S) (Cell Signaling Technology, Danvers, MA, USA), or anti-p300 (sc-48343), anti-MAP2 (sc-20172) (Santa Cruz Biotechnology, Santa Cruz, CA, USA), or anti-HSC70 (ab51052), and anti-LAMP2A (ab18528) (Abcam, Cambridge, MA, USA) at 4°C overnight, followed by incubation with Alexa Fluor secondary antibodies (Thermo Fisher Scientific, Waltham, MA, USA) for 2 hours at room temperature. Subsequently, the cells were stained with 4′,6-diamidino-2-phenylindole (DAPI) (Sigma-Aldrich) for 5 min and then washed three times with PBS. Last, the cells were observed with a confocal microscope system (Nikon, Tokyo, Japan).

CM assays

The procedure of CM assays has been previously described (*35*). Briefly, BV2 cells or primary microglia were pretreated with or without CA for 12 hours, followed by PBS or LPS for 6 hours. The cells were washed twice and cultured with fresh culture medium for 24 hours. After treatments, the CM from BV2 cells or primary microglia were collected to culture SH-SY5Y cells or primary cortical neurons for 24 hours for further assays.

PI staining assay

SH-SY5Y cells were cultured with microglial CM for 24 hours. Then, the cells were incubated with Hoechst 33342 (Sigma-Aldrich, St. Louis, MO, USA) and PI (Sigma-Aldrich, St. Louis, MO, USA) for 5 min. Then, the cells were observed with an inverted IX71 microscope system (Olympus, Tokyo, Japan).

Immunohistochemistry

After the treatments with CA and LPS described above, the mice were anesthetized with pentobarbital sodium (40 mg/ml) and then perfused with 40 ml of PBS, followed by 20 ml of 4% PFA in 0.1 M PBS (pH 7.4). Next, the brains were removed and postfixed in the same fixation agent at 4°C for 3 days. After fixation, the brains were treated with 30% sucrose at 4°C for another 3 days. A freezing microtome (Leica CM1950, Leica Biosystems, Nussloch, DEU) was used to cut the brains into 20-μm-thick slices. Immunocytochemistry staining was performed with primary antibodies: anti-TH (25648S) (Cell Signaling Technology, Danvers, MA, USA), anti-IBA1 (019-19741) (Wako Chemicals, Tokyo, Japan), and anti-GFAP (MAB360) (Millipore, Billerica, MA, USA) at 4°C overnight. Then, the slices were incubated with Alexa Fluor secondary antibodies for 2 hours at room temperature. Last, after incubation with DAPI, all slices were observed with an inverted IX71 microscope system (Olympus, Tokyo, Japan).

Statistical analysis

The quantification analysis of immunoblots was performed using Photoshop 7.0 (Adobe, San Jose, CA, USA). GraphPad Prism 7.00 (GraphPad Software, version X; La Jolla, CA, USA) was used for statistical analysis and graphing. Significant differences were evaluated using unpaired *t* test, one-way or two-way analysis of variance (ANOVA) followed by Dunnett′s or Tukey′s multiple comparisons test. The criterion of significance was set at $P < 0.05$. $^{*}P < 0.05$, $^{**}P < 0.01$, and $^{***}P < 0.001$; ns indicates no significant difference. The values are shown as the means ± SD.

Supplementary Materials

This PDF file includes:

Figs. S1 to S5

REFERENCES AND NOTES

1. B. R. Bloem, M. S. Okun, C. Klein, Parkinson's disease. *Lancet* **397**, 2284–2303 (2021).
2. R. Wang, H. Sun, H. Ren, G. Wang, α-Synuclein aggregation and transmission in Parkinson's disease: A link to mitochondria and lysosome. *Sci. China Life Sci.* **63**, 1850–1859 (2020).
3. Y. C. Wong, D. Krainc, α-synuclein toxicity in neurodegeneration: Mechanism and therapeutic strategies. *Nat. Med.* **23**, 1–13 (2017).
4. M. J. Armstrong, M. S. Okun, Diagnosis and treatment of Parkinson disease: A review. *JAMA* **323**, 548–560 (2020).
5. D. Aarsland, L. Batzu, G. M. Halliday, G. J. Geurtsen, C. Ballard, K. Ray Chaudhuri, D. Weintraub, Parkinson disease-associated cognitive impairment. *Nat. Rev. Dis. Primers* **7**, 47 (2021).
6. P. Garcia, W. Jürgens-Wemheuer, O. Uriarte Huarte, A. Michelucci, A. Masuch, S. Brioschi, A. Weihofen, E. Koncina, D. Coowar, T. Heurtaux, E. Glaab, R. Balling, C. Sousa, T. Kaoma, N. Nicot, T. Pfander, W. Schulz-Schaeffer, A. Allouche, N. Fischer, K. Biber, F. Kleine-Borgmann, M. Mittelbronn, M. Ostaszewski, K. J. Schmit, M. Buttini, Neurodegeneration and neuroinflammation are linked, but independent of α -synuclein inclusions, in a seeding/spreading mouse model of Parkinson's disease. *Glia* **70**, 935–960 (2022).
7. A. Gerhard, N. Pavese, G. Hotton, F. Turkheimer, M. Es, A. Hammers, K. Eggert, W. Oertel, R. B. Banati, D. J. Brooks, In vivo imaging of microglial activation with [^{11}C](R)-PK11195 PET in idiopathic Parkinson's disease. *Neurobiol. Dis.* **21**, 404–412 (2006).
8. M. G. Tansey, R. L. Wallings, M. C. Houser, M. K. Herrick, C. E. Keating, V. Joers, Inflammation and immune dysfunction in Parkinson disease. *Nat. Rev. Immunol.* **22**, 657–673 (2022).
9. K. Imamura, N. Hishikawa, M. Sawada, T. Nagatsu, M. Yoshida, Y. Hashizume, Distribution of major histocompatibility complex class II-positive microglia and cytokine profile of Parkinson's disease brains. *Acta Neuropathol.* **106**, 518–526 (2003).
10. C. Gu, F. Wang, Y.-T. Zhang, S.-Z. Wei, J.-Y. Liu, H.-Y. Sun, G.-H. Wang, C.-F. Liu, Microglial MT1 activation inhibits LPS-induced neuroinflammation via regulation of metabolic reprogramming. *Aging Cell* **20**, e13375 (2021).
11. X.-W. Zhang, N. Feng, Y.-C. Liu, Q. Guo, J.-K. Wang, Y.-Z. Bai, X.-M. Ye, Z. Yang, H. Yang, Y. Liu, M.-M. Yang, Y.-H. Wang, X.-M. Shi, D. Liu, P.-F. Tu, K.-W. Zeng, Neuroinflammation inhibition by small-molecule targeting USP7 noncatalytic domain for neurodegenerative disease therapy. *Sci. Adv.* **8**, eabo0789 (2022).
12. A. Ghosh, A. Roy, X. Liu, J. H. Kordower, E. J. Mufson, D. M. Hartley, S. Ghosh, R. L. Mosley, H. E. Gendelman, K. Pahan, Selective inhibition of NF-κB activation prevents dopaminergic neuronal loss in a mouse model of Parkinson's disease. *Proc. Natl. Acad. Sci. U.S.A.* **104**, 18754–18759 (2007).

13. D. Dutta, M. Jana, M. Majumder, S. Mondal, A. Roy, K. Pahan, Selective targeting of the TLR2/MyD88/NF-κB pathway reduces α-synuclein spreading in vitro and in vivo. *Nat. Commun.* **12**, 5382 (2021).
14. I. Choi, Y. Zhang, S. P. Seegobin, M. Pruvost, Q. Wang, K. Purtell, B. Zhang, Z. Yue, Microglia clear neuron-released α-synuclein via selective autophagy and prevent neurodegeneration. *Nat. Commun.* **11**, 1386 (2020).
15. A. Oeckinghaus, M. S. Hayden, S. Ghosh, Crosstalk in NF-κB signaling pathways. *Nat. Immunol.* **12**, 695–708 (2011).
16. Y. He, H. Hara, G. Núñez, Mechanism and regulation of NLRP3 inflammasome activation. *Trends Biochem. Sci.* **41**, 1012–1021 (2016).
17. H. L. Chiang, S. R. Terlecky, C. P. Plant, J. F. Dice, A role for a 70-kilodalton heat shock protein in lysosomal degradation of intracellular proteins. *Science* **246**, 382–385 (1989).
18. J. F. Dice, Peptide sequences that target cytosolic proteins for lysosomal proteolysis. *Trends Biochem. Sci.* **15**, 305–309 (1990).
19. A. M. Cuervo, J. F. Dice, A receptor for the selective uptake and degradation of proteins by lysosomes. *Science* **273**, 501–503 (1996).
20. S. Kaushik, A. M. Cuervo, AMPK-dependent phosphorylation of lipid droplet protein PLIN2 triggers its degradation by CMA. *Autophagy* **12**, 432–438 (2016).
21. A. M. Cuervo, E. Knecht, S. R. Terlecky, J. F. Dice, Activation of a selective pathway of lysosomal proteolysis in rat liver by prolonged starvation. *Am. J. Physiol.* **269**, C1200–C1208 (1995).
22. E. Dohi, S. Tanaka, T. Seki, T. Miyagi, I. Hide, T. Takahashi, M. Matsumoto, N. Sakai, Hypoxic stress activates chaperone-mediated autophagy and modulates neuronal cell survival. *Neurochem. Int.* **60**, 431–442 (2012).
23. W. Li, J. Zhu, J. Dou, H. She, K. Tao, H. Xu, Q. Yang, Z. Mao, Phosphorylation of LAMP2A by p38 MAPK couples ER stress to chaperone-mediated autophagy. *Nat. Commun.* **8**, 1763 (2017).
24. A. M. Cuervo, L. Stefanis, R. Fredenburg, P. T. Lansbury, D. Sulzer, Impaired degradation of mutant α-synuclein by chaperone-mediated autophagy. *Science* **305**, 1292–1295 (2004).
25. M. Bourdenx, A. Martín-Segura, A. Scrivo, J. A. Rodriguez-Navarro, S. Kaushik, I. Tasset, A. Diaz, N. J. Storm, Q. Xin, Y. R. Juste, E. Stevenson, E. Luengo, C. C. Clement, S. J. Choi, N. J. Krogan, E. V. Mosharov, L. Santambrogio, F. Grueninger, L. Collin, D. L. Swaney, D. Sulzer, E. Gavathiotis, A. M. Cuervo, Chaperone-mediated autophagy prevents collapse of the neuronal metastable proteome. *Cell* **184**, 2696–2714.e25 (2021).
26. T. Vogiatzi, M. Xilouri, K. Vekrellis, L. Stefanis, Wild type α-synuclein is degraded by chaperone-mediated autophagy and macroautophagy in neuronal cells. *J. Biol. Chem.* **283**, 23542–23556 (2008).
27. S. J. Orenstein, S.-H. Kuo, I. Tasset, E. Arias, H. Koga, I. Fernandez-Carasa, E. Cortes, L. S. Honig, W. Dauer, A. Consiglio, A. Raya, D. Sulzer, A. M. Cuervo, Interplay of LRRK2 with chaperone-mediated autophagy. *Nat. Neurosci.* **16**, 394–406 (2013).
28. B. Wang, Z. Cai, K. Tao, W. Zeng, F. Lu, R. Yang, D. Feng, G. Gao, Q. Yang, Essential control of mitochondrial morphology and function by chaperone-mediated autophagy through degradation of PARK7. *Autophagy* **12**, 1215–1228 (2016).
29. K. E. Murphy, A. M. Gysbers, S. K. Abbott, A. S. Spiro, A. Furuta, A. Cooper, B. Garner, T. Kabuta, G. M. Halliday, Lysosomal-associated membrane protein 2 isoforms are differentially affected in early Parkinson's disease. *Mov. Disord.* **30**, 1639–1647 (2015).
30. N. Papagiannakis, M. Xilouri, C. Koros, M. Stamelou, R. Antonelou, M. Maniati, D. Papadimitriou, M. Moraitou, H. Michelakakis, L. Stefanis, Lysosomal alterations in peripheral blood mononuclear cells of Parkinson's disease patients. *Mov. Disord.* **30**, 1830–1834 (2015).
31. M. Xilouri, O. R. Brekk, N. Landeck, P. M. Pitychoutis, T. Papasilekas, Z. Papadopoulou-Daifoti, D. Kirik, L. Stefanis, Boosting chaperone-mediated autophagy in vivo mitigates α-synuclein-induced neurodegeneration. *Brain* **136**, 2130–2146 (2013).
32. T. Nie, K. Tao, L. Zhu, L. Huang, S. Hu, R. Yang, P. Xu, Z. Mao, Q. Yang, Chaperone-mediated autophagy controls the turnover of E3 ubiquitin ligase MARCHF5 and regulates mitochondrial dynamics. *Autophagy* **17**, 2923–2938 (2021).
33. J.-Z. Wu, M. Ardah, C. Haikal, A. Svanbergsson, M. Diepenbroek, N. N. Vaikath, W. Li, Z.-Y. Wang, T. F. Outeiro, O. M. El Agnaf, J.-Y. Li, Dihydromyricetin and Salvianolic acid B inhibit α-synuclein aggregation and enhance chaperone-mediated autophagy. *Transl. Neurodegener.* **8**, 18 (2019).
34. J. Zhang, J. L. Johnson, J. He, G. Napolitano, M. Ramadass, C. Rocca, W. B. Kiosses, C. Bucci, Q. Xin, E. Gavathiotis, A. M. Cuervo, S. Cherqui, S. D. Catz, Cystinosin, the small GTPase Rab11, and the Rab7 effector RILP regulate intracellular trafficking of the chaperone-mediated autophagy receptor LAMP2A. *J. Biol. Chem.* **292**, 10328–10346 (2017).
35. H. Sun, J. Wu, R. Wang, S. Zhang, H. Xu, E. Kaznacheyeva, X. Lu, H. Ren, G. Wang, Pazopanib alleviates neuroinflammation and protects dopaminergic neurons in LPS-stimulated mouse model by inhibiting MEK4-JNK-AP-1 pathway. *Acta Pharmacol. Sin.* **44**, 1135–1148 (2023).
36. C. Gu, Q. Hu, J. Wu, C. Mu, H. Ren, C.-F. Liu, G. Wang, P7C3 inhibits lps-induced microglial activation to protect dopaminergic neurons against inflammatory factor-induced cell death in vitro and in vivo. *Front. Cell. Neurosci.* **12**, 400 (2018).
37. A. Dong, Y. Yang, S. Jiang, X. Yao, D. Qi, C. Mao, X. Cheng, F. Wang, L. Hu, C. Liu, Pramipexole inhibits astrocytic NLRP3 inflammasome activation via Drd3-dependent autophagy in a mouse model of Parkinson's disease. *Acta Pharmacol. Sin.* **44**, 32–43 (2023).
38. J. Peng, J. Li, J. Huang, P. Xu, H. Huang, Y. Liu, L. Yu, Y. Yang, B. Zhou, H. Jiang, K. Chen, Y. Dang, Y. Zhang, C. Luo, G. Li, p300/CBP inhibitor A-485 alleviates acute liver injury by regulating macrophage activation and polarization. *Theranostics* **9**, 8344–8361 (2019).
39. L. Chen, Y. Mu, W. C. Greene, Acetylation of RelA at discrete sites regulates distinct nuclear functions of NF-κB. *EMBO J.* **21**, 6539–6548 (2002).
40. L. Chen, W. Fischle, E. Verdin, W. C. Greene, Duration of nuclear NF-κB Action regulated by reversible acetylation. *Science* **293**, 1653–1657 (2001).
41. L. Gao, H. She, W. Li, J. Zeng, J. Zhu, D. P. Jones, Z. Mao, G. Gao, Q. Yang, Oxidation of survival factor MEF2D in neuronal death and parkinson's disease. *Antioxid. Redox Signal.* **20**, 2936–2948 (2014).
42. P. Kirchner, M. Bourdenx, J. Madrigal-Matute, S. Tiano, A. Diaz, B. A. Bartholdy, B. Will, A. M. Cuervo, Proteome-wide analysis of chaperone-mediated autophagy targeting motifs. *PLOS Biol.* **17**, e3000301 (2019).
43. S. A. Wolf, H. W. G. M. Boddeke, H. Kettenmann, Microglia in physiology and disease. *Annu. Rev. Physiol.* **79**, 619–643 (2017).
44. R. Gomez-Sintes, Q. Xin, J. I. Jimenez-Loygorri, M. McCabe, A. Diaz, T. P. Garner, X. M. Cotto-Rios, Y. Wu, S. Dong, C. A. Reynolds, B. Patel, P. de la Villa, F. Macian, P. Boya, E. Gavathiotis, A. M. Cuervo, Targeting retinoic acid receptor α-corepressor interaction activates chaperone-mediated autophagy and protects against retinal degeneration. *Nat. Commun.* **13**, 4220 (2022).
45. M. Martinez-Vicente, Z. Talloczy, S. Kaushik, A. C. Massey, J. Mazzulli, E. V. Mosharov, R. Hodara, R. Fredenburg, D. C. Wu, A. Follenzi, W. Dauer, S. Przedborski, H. Ischiropoulos, P. T. Lansbury, D. Sulzer, A. M. Cuervo, Dopamine-modified α-synuclein blocks chaperone-mediated autophagy. *J. Clin. Invest.* **118**, 777–788 (2008).
46. P. W.-L. Ho, C.-T. Leung, H. Liu, S. Y.-Y. Pang, C. S.-C. Lam, J. Xian, L. Li, M. H.-W. Kung, D. B. Ramsden, S.-L. Ho, Age-dependent accumulation of oligomeric SNCA/α-synuclein from impaired degradation in mutant LRRK2 knockin mouse model of Parkinson disease: Role for therapeutic activation of chaperone-mediated autophagy (CMA). *Autophagy* **16**, 347–370 (2020).
47. R. Valdor, E. Mocholi, Y. Botbol, I. Guerrero-Ros, D. Chandra, H. Koga, C. Gravekamp, A. M. Cuervo, F. Macian, Chaperone-mediated autophagy regulates T-cell responses through targeted degradation of negative regulators of T-cell activation. *Nat. Immunol.* **15**, 1046–1054 (2014).
48. L. Qiao, J. Ma, Z. Zhang, W. Sui, C. Zhai, D. Xu, Z. Wang, H. Lu, M. Zhang, C. Zhang, W. Chen, Y. Zhang, Deficient chaperone-mediated autophagy promotes inflammation and atherosclerosis. *Circ. Res.* **129**, 1141–1157 (2021).
49. J. Chen, K. Mao, H. Yu, Y. Wen, H. She, H. Zhang, L. Liu, M. Li, W. Li, F. Zou, p38-TFEB pathways promote microglia activation through inhibiting CMA-mediated NLRP3 degradation in Parkinson's disease. *J. Neuroinflammation* **18**, 295 (2021).
50. M. Zhang, S. Y. Tian, S. Y. Ma, X. Zhou, X. H. Zheng, B. Li, G. Y. Guo, J. H. Yu, R. Su, F. F. Yang, Y. N. Hu, G. Ma, H. Yang, L. H. Zheng, C. C. Guo, Y. L. Shang, J. B. Wang, Y. Han, Deficient chaperone-mediated autophagy in macrophage aggravates inflammation of nonalcoholic steatohepatitis by targeting Nup85. *Liver Int.* **43**, 1021–1034 (2023).
51. L. A. J. O'Neill, D. Golenbock, A. G. Bowie, The history of Toll-like receptors—Redefining innate immunity. *Nat. Rev. Immunol.* **13**, 453–460 (2013).
52. J. Zhang, J. Huang, Y. Gu, M. Xue, F. Qian, B. Wang, W. Yang, H. Yu, Q. Wang, X. Guo, X. Ding, J. Wang, M. Jin, Y. Zhang, Inflammation-induced inhibition of chaperone-mediated autophagy maintains the immunosuppressive function of murine mesenchymal stromal cells. *Cell. Mol. Immunol.* **18**, 1476–1488 (2021).
53. J. Tang, M.-N. Zhan, Q.-Q. Yin, C.-X. Zhou, C.-L. Wang, L.-L. Wo, M. He, G.-Q. Chen, Q. Zhao, Impaired p65 degradation by decreased chaperone-mediated autophagy activity facilitates epithelial-to-mesenchymal transition. *Oncogenesis* **6**, e387 (2017).
54. H. Zhong, M. J. May, E. Jimi, S. Ghosh, The phosphorylation status of nuclear NF-κB determines its association with CBP/p300 or HDAC-1. *Mol. Cell* **9**, 625–636 (2002).
55. A. Duran, M. T. Diaz-Meco, J. Moscat, Essential role of RelA Ser311 phosphorylation by ζPKC in NF-κB transcriptional activation. *EMBO J.* **22**, 3910–3918 (2003).
56. L.-F. Chen, W. C. Greene, Shaping the nuclear action of NF-κB. *Nat. Rev. Mol. Cell Biol.* **5**, 392–401 (2004).
57. X. Xu, J. Li, X. Long, S. Tao, X. Yu, X. Ruan, K. Zhao, L. Tian, C646 protects against DSS-induced colitis model by targeting NLRP3 inflammasome. *Front. Pharmacol.* **12**, 707610 (2021).

58. C. Du, D. Huang, Y. Peng, Y. Yao, Y. Zhao, Y. Yang, H. Wang, L. Cao, W.-G. Zhu, J. Gu, 5-Fluorouracil targets histone acetyltransferases p300/CBP in the treatment of colorectal cancer. *Cancer Lett.* **400**, 183–193 (2017).
59. W. Wan, Z. You, Y. Xu, L. Zhou, Z. Guan, C. Peng, C. C. L. Wong, H. Su, T. Zhou, H. Xia, W. Liu, mTORC1 phosphorylates acetyltransferase p300 to regulate autophagy and lipogenesis. *Mol. Cell* **68**, 323–335.e6 (2017).
60. C. Park, Y. Suh, A. M. Cuervo, Regulated degradation of Chk1 by chaperone-mediated autophagy in response to DNA damage. *Nat. Commun.* **6**, 6823 (2015).
61. S. Zhang, B. Hu, Y. You, Z. Yang, L. Liu, H. Tang, W. Bao, Y. Guan, X. Shen, Sorting nexin 10 acts as a tumor suppressor in tumorigenesis and progression of colorectal cancer through regulating chaperone mediated autophagy degradation of $p21^{Cip1/WAF1}$. *Cancer Lett.* **419**, 116–127 (2018).
62. Y. He, X. Yao, N. Taylor, Y. Bai, T. Lovenberg, A. Bhattacharya, RNA sequencing analysis reveals quiescent microglia isolation methods from postnatal mouse brains and limitations of BV2 cells. *J. Neuroinflammation* **15**, 153 (2018).
63. M. Xilouri, O. R. Brekk, A. Polissidis, M. Chrysanthou-Piterou, I. Kloukina, L. Stefanis, Impairment of chaperone-mediated autophagy induces dopaminergic neurodegeneration in rats. *Autophagy* **12**, 2230–2247 (2016).
64. Z. Hao, L. Liu, Z. Tao, R. Wang, H. Ren, H. Sun, Z. Lin, Z. Zhang, C. Mu, J. Zhou, G. Wang, Motor dysfunction and neurodegeneration in a *C9orf72* mouse line expressing poly-PR. *Nat. Commun.* **10**, 2906 (2019).
65. Q. Xia, Q. Hu, H. Wang, H. Yang, F. Gao, H. Ren, D. Chen, C. Fu, L. Zheng, X. Zhen, Z. Ying, G. Wang, Induction of COX-2-PGE2 synthesis by activation of the MAPK/ERK pathway contributes to neuronal death triggered by TDP-43-depleted microglia. *Cell Death Dis.* **6**, e1702 (2015).
66. A. C. Massey, S. Kaushik, G. Sovak, R. Kiffin, A. M. Cuervo, Consequences of the selective blockage of chaperone-mediated autophagy. *Proc. Natl. Acad. Sci. U.S.A.* **103**, 5805–5810 (2006).
67. Y. Xu, Y. Zhang, J. C. García-Cañaveras, L. Guo, M. Kan, S. Yu, I. A. Blair, J. D. Rabinowitz, X. Yang, Chaperone-mediated autophagy regulates the pluripotency of embryonic stem cells. *Science* **369**, 397–403 (2020).

Acknowledgments: We are grateful to J. Ding (Renji Hospital, Shanghai Jiao Tong University) for providing the BV2 cells. We thank J. Xu (Institute of Neuroscience, Chinese Academy of Sciences) for the SH-SY5Y cells. We also thank Y. Xu (Cambridge-Suda Genomic Resource Center, Soochow University) for the U2OS cells. **Funding:** This work was supported by the National Natural Science Foundation of China (grants 32261133525, 32271039, 32070970, and 31970966) and the Priority Academic Program Development of Jiangsu Higher Education Institutions from Jiangsu Education Department. **Author contributions:** J.W. and G.W. designed the study. J.W. performed most of the experiments. Y.H., H.X., H.S., and R.W. performed some of the biochemical and cellular experiments. J.W. and H.R. analyzed the data. J.W. drafted the manuscript. H.R. and G.W. revised the manuscript. All authors read and approved the manuscript. **Competing interests:** The authors declare that they have no competing interests. **Data and materials availability:** All data needed to evaluate the conclusions in the paper are present in the paper and/or the Supplementary Materials.

Submitted 21 May 2023
Accepted 6 September 2023
Published 6 October 2023
10.1126/sciadv.adi8343